NASA CR-134985
PWA-5329

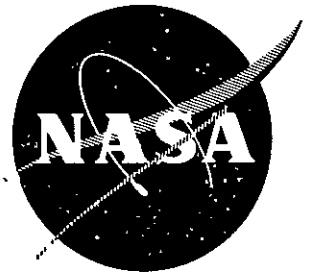

IMPROVED TURBINE DISK DESIGN TO INCREASE RELIABILITY OF AIRCRAFT JET ENGINES

By A. S. Alver
J K. Wong

PRATT & WHITNEY AIRCRAFT DIVISION
UNITED TECHNOLOGIES CORPORATION

prepared for

NATIONAL AERONAUTICS AND SPACE ADMINISTRATION

NASA Lewis Research Center
Contract NAS3-18558

1 Report No	2 Government Accession No	3 Recipient's Catalog No
NASA CR-134985		

4 Title and Subtitle	5 Report Date
IMPROVED TURBINE DISK DESIGN TO INCREASE RELIABILITY OF AIRCRAFT JET ENGINES	October 1975
	6 Performing Organization Code

7 Author(s)	8 Performing Organization Report No
A. S. Alver and J K Wong	PWA-5329
	10 Work Unit No

9 Performing Organization Name and Address	11 Contract or Grant No
Pratt & Whitney Aircraft Division United Technologies Corporation East Hartford, Connecticut 06108	NAS3-18558
	13 Type of Report and Period Covered
12 Sponsoring Agency Name and Address	Contractor Report
National Aeronautics and Space Administration Washington, D C 20546	14 Sponsoring Agency Code

15 Supplementary Notes

Project Manager, Albert Kaufman, Fluid System Components Division, NASA Lewis Research Center, Cleveland, Ohio

16 Abstract

An analytical study was conducted on a bore-entry-cooled turbine disk for the first stage of the JT8D-17 high pressure turbine which had the potential to improve disk life over the existing Bill of Material design The disk analysis included the consideration of transient and steady-state temperature, blade loading, creep, low cycle fatigue, fracture mechanics and manufacturing flaws The approach adopted in the study was to increase the cyclic life of the turbine disk without increasing the disk weight over the Bill of Material disk, while maintaining engine performance. The improvement in life of the bore-entry-cooled turbine disk was determined by comparing it with the existing disk made of both conventional (Waspaloy®) and advanced (Astroloy) disk materials. The improvement in crack initiation life of the Astroloy bore-entry-cooled disk is 87% and 67% over the existing disk made of Waspaloy® and Astroloy, respectively. Improvement in crack propagation life is 124% over the Waspaloy® and 465% over the Astroloy disks. The available kinetic energies of disk fragments calculated for the three disks indicate a lower fragment energy level for the bore-entry-cooled turbine disk.

17 Key Words (Suggested by Author(s))	18 Distribution Statement
High pressure turbine disk Bonded disk Bore-entry-cooled disk Turbine disk fragment energy Turbine disk life improvement	

19 Security Classif (of this report)	20 Security Classif (of this page)	21 No of Pages	22 Price*
Unclassified	Unclassified	64	

* For sale by the National Technical Information Service, Springfield, Virginia 22151

TABLE OF CONTENTS

LIST OF ILLUSTRATIONS

LIST OF ILLUSTRATIONS (Cont'd)

LIST OF TABLES

SUMMARY

Pratt & Whitney Aircraft conducted a nine month program, under NASA contract NAS3-18558, to study an advanced turbine disk design concept. The objectives of the "Improved Turbine Disk Design to Increase Reliability of Aircraft Jet Engines" program were to design a new turbine disk (referred to as the design disk) which could be a potential replacement for the existing first-stage turbine disk in the JT8D-17 commercial turbofan aircraft engine, and conduct the analysis necessary to calculate the improvement in disk life and overspeed capability resulting from the new design.

The design disk studied under this program was a bore-entry-cooled bonded disk In the bore-entry-cooled concept, turbine blade cooling air is introduced at the disk bore, pumped radially through internal channels in the disk (one for each turbine blade) and exits to supply the blades at the blade attachment slot at the disk rim. The disk is fabricated in halves in which the cooling air channels are machined. The two disk halves are bonded together at the radial vanes between the cooling channels and at the disk rim using a transient liquid phase (TLP®) bond

A simplified JT8D-17 engine flight cycle was used in the disk analysis which included consideration of transient and steady-state temperature, blade loading, creep, low cycle fatigue, fracture mechanics, and manufacturing flaws The design conditions and criteria that went into the design of the existing first-stage high pressure turbine disk for the JT8D-17 turbofan engine were used in the study of the design disk. The same analytical methods were used where applicable in the calculation of temperatures, stresses, and lives for the standard (Bill of Material), advanced standard (Bill of Material disk geometry with material changed from Waspaloy® to an advanced material, Astroloy) and design disks. The design disk has no deleterious effect on the engine performance as compared to performance obtained with the existing turbine disk. The turbine blade airfoil, and the amount and temperature of the blade coolant were the same as used in the present JT8D-17 engine The diametral growth due to creep of the design disk prior to failure does not exceed that of the standard disk, since the disks are not creep limited The limiting low cycle fatigue (LCF) crack initiation lives of the standard, advanced standard and design disks are 16,000, 18,000 and 30,000 cycles, respectively, and the crack propagation lives are 2900, 1150 and 6500 cycles, respectively. The improvement in life of the initially unflawed design disk over the initially unflawed standard and advanced standard disks is 93% and 90%, respectively, obtained by comparing the total of the number of cycles to crack initiation and the number of cycles during the crack propagation period. The limiting life location in all three disks is at the LCF crack initiation site of the disk. The increase in the crack propagation life for the LCF crack initiated flawed design disk is 465% over the advanced standard disk and 124% over the standard disk. The weight of the Astroloy design disk is the same as that of the existing Waspaloy® standard disk. The overspeed capability, or burst margin, established by comparing disk burst speed to the maximum speed of the engine for the standard, advanced standard and design disks are 35.6%, 35.9% and 33%, respectively; and they are all above the design minimum of 22%.

Based on disk fracture experience, available kinetic energies of assumed disk fragments were calculated for the three disks. The results indicated smaller fragments and hence lower fragment energies for the design disk as compared to the standard and advanced standard disks.

1.0 INTRODUCTION

1.1 BACKGROUND

A disk burst is potentially the most catastrophic failure possible in an engine and thus disks are designed with overspeed capability and low cycle fatigue life as primary objectives The requirement for higher turbine stage work without additional stages has resulted in increased turbine blade tip speeds and higher turbine inlet temperatures in advanced commercial engines. This trend has resulted in significant increases in turbine stage disk rim loading and a more severe thermal environment, thereby making it more difficult to design turbine disks for specified life requirements meeting current weight goals Indications are that both turbine blade tip speeds and turbine inlet temperatures will continue to increase in advanced commercial engines as higher turbine work levels are achieved. Advanced turbine disk concepts are required to insure long life disks in commercial engines considering both crack initiation and propagation, without resulting in severe weight, performance, or cost penalties.

1.2 PROGRAM

The goal of the "Improved Turbine Disk Design to Increase Reliability of Aircraft Jet Engines" program was to design an advanced concept turbine disk which could be a potential replacement for a Bill-of-Material first-stage turbine disk in an existing commercial engine and which would have improved reliability with respect to the Bill-of-Material disk. P&WA's approach to achieve the program goal was to increase the cycle life of the turbine disk without increasing the disk weight, while maintaining engine performance.

The Pratt & Whitney Aircraft JT8D-17 turbofan engine was selected as the study vehicle for the improved turbine disk life program. The -17 model is the latest and most advanced version of the JT8D engine which is the most widely used commercial jet engine, supplying power to 45 percent of the world's commercial fleet. The JT8D has been in commercial service for 10 years and over 71,000,000 total engine hours have been accumulated on over 6,600 delivered engines. The current rate of use is approximately 1,000,000 hours and 1,000,000 cycles per month.

Over the years, engine model changes have been incorporated to increase thrust from the original 62,300 newtons (14,000 pounds) for the JT8D-1 to 71,200 newtons (16,000 pounds) for the JT8D-17. Turbine inlet temperatures have increased 140°K (260°F). The use of air-cooled first-stage turbine blades was initiated with the JT8D-11 model, and approximately 1300 engines with air-cooled turbine blades have been delivered, of which 235 are the JT8D-17 model. Engineering development to further improve the JT8D will continue for the remainder of this decade. The disk concept studied in this program is applicable to this type of engine in service today and advanced commercial engines.

Pratt & Whitney Aircraft conducted a 9 month analytical study of three first-stage turbine disks for the JT8D-17 engine. The first disk, called the "standard" disk, is the Bill-of-Material (B/M) Waspaloy® JT8D-17 first-stage high pressure turbine disk. The second disk, called the "advanced standard" disk, is a disk with a geometry identical to that of the B/M disk, but made of an advanced material, Astroloy The third disk is the "design" disk which

is a bore-entry-cooled, transient liquid phase (ref. 1) bonded disk, made of Astroloy. The reason for the three disks was to separate the life improvement in the design disk due to the advanced structural concept from the life improvement obtained through the use of an advanced disk material. In the study, the same design conditions, criteria, and engine flight cycle were used for the three disks, and the same analytical methods were used where applicable The disk analysis included considerations of transient and steady-state temperature, blade loading, creep, low cycle fatigue, fracture mechanics, and manufacturing flaws

The improvement in life of the design disk was compared to that of the standard and advanced standard disks. Comparisons were made on the basis of cycles to crack initiation and over-speed capability for initially unflawed disks and on the basis of failure for initially flawed disks. Available kinetic energies of disk fragments for the three disks were also calculated and compared.

Ref. 1 Duvall, D S, Owczarski, W. A, and Paulonis, D F, "TLP® Bonding A New Method for Joining Heat Resistant Alloys," Welding Journal, April 1974, p. 203-214.

2.0 DISK DESIGN

The existing first-stage turbine disk, or standard disk, for the JT8D-17 turbofan engine is shown in Figure 1. Cooling of the high pressure turbine blades is accomplished using compressor discharge air delivered by a conventional tangential on-board injection (TOBI) system. The TOBI turbine rotor cooling air delivery system bleeds high compressor discharge air from the combustion chamber liner and projects this air onto the turbine disk. Work is extracted from the bleed air by trading the higher than required compressor discharge pressure for tangential velocity produced in the TOBI nozzles. That is, the high tangential momentum produced by TOBI nozzles does work on the conventional turbine disk in the same manner as an impulse turbine. The work accomplished on the disk reduces both the temperature and pressure of the turbine rotor cooling air as it flows to the turbine airfoils. It is important to note that with the TOBI delivery the cooling air is raised to a higher pressure (i e., more compressor work) than required for turbine airfoil cooling and then pressure is lowered to the airfoil requirement by the removal of work (i e , TOBI work). Each of the 80 turbine blades is then fed air through a drilled hole which delivers air from the point of on-board injection, through the disk rim to the bottom of the blade attachment slot below the blade. The opening of the angled cooling air hole in the disk rim broach results in an elliptical exit opening with high stress concentration and is the limiting low cycle fatigue life location in the standard disk. The advanced standard disk is identical to the standard disk except for a disk material change from Waspaloy® to an advanced material, Astroloy. The design disk, which has the potential to replace the existing first-stage turbine disk in the JT8D-17 engine, is a bore-entry-cooled, bonded disk

The bore-entry cooled disk concept entails bleeding the turbine cooling air inboard at the mid-compressor and transferring the air axially between the high and low turbine shafts to the bonded disk bore where it is pumped up through the disk in carefully designed internal channels, one for each turbine blade, and exits to supply the blade attachment slot at the disk rim as shown in Figure 2.

Cooling air arriving at the airfoils in this manner has not been pumped to higher pressures than required for turbine airfoil requirements. That is , compressor work above that required to reach turbine airfoil pressure has not been added to and removed from the cooling air Thus, cooling air arriving at the turbine airfoils in this manner requires less compressor work than conventional TOBI systems. The amount of heat picked up by the cooling air as it passes through the radial air channels in the design disk is small and thus no additional coolant is needed to cool the turbine blades at the disk rim.

Tailoring the design of the blade cooling air radial pumping passages yields control of the disk radial thermal gradient even during engine transients. The disk is fabricated in halves in which the cooling air channels are machined The two disk halves are bonded together at the radial vanes between the cooling channels and at the disk rim using transient liquid phase (TLP®) bonding

2.1 DESIGN CONSIDERATIONS/CONDITIONS/CRITERIA

The design conditions and criteria used in the design of the existing first-stage high pressure turbine disk for the JT8D-17 turbofan engine were also used for the design disk. The simplified JT8D-17 engine flight cycle used for the analysis of the standard, advanced standard, and design disks is shown in Figure 3 in terms of altitude, inlet Mach number, turbine inlet temperature, and engine speed versus flight time.

The design disk has no deleterious effect on the engine performance as compared to performance obtained with the existing Bill-of-Material standard disk Neither the turbine blade airfoil nor the amount or temperature of the blade coolant in the present engine was changed. Provision was made in the disk design for channeling coolant to the blades The diametral growth due to creep of the design disk prior to failure does not exceed that of the standard disk, since the disks are not creep limited The design properties of Astroloy, the advanced disk material used in the analysis of the advanced standard and design disks, are shown in Figure 4. The design properties of Waspaloy used in the analysis of the standard disk are shown in Figure 5

The configuration of the design disk, in regard to provisions for supplying cooling air to the blades, which was required for the calculation of transient and steady-state radial and axial temperatures was accomplished by introducing turbine blade cooling air into the disk bore/shaft annulus. Radial air passage channels in the design disk then pump the turbine cooling air from the disk bore to the blade supplying the required pressure at the disk rim (Figure 2) To minimize the pressure losses associated with entrance, friction and turning experienced by the cooling air in the annular passage between the design disk bore and the engine shaft, the design disk bore radius was moved outward 0 25 cm (0 10 inch) relative to the standard and advanced standard designs. This set the minimum bore diameter of the design disk at 12.0 cm (4.70 inches) versus 11 43 cm (4.50 inches) for the existing JT8D-17 first-stage high pressure turbine disk and the advanced standard disk The rim diameter of the design disk is the same as that in the standard and advanced standard disk since all three disks are designed to use the same turbine blade airfoil, blade attachment, disk broach slot and disk sideplate configuration The radial air passages necessary to achieve the required blade supply pressure at the design disk rim while having no deleterious effect on the engine performance are shown in Figure 6.

2.2 DESIGN ANALYSIS

In the calculation of temperatures, stresses, and lives for the standard, advanced standard, and design disks, the same analytical methods were used where applicable. The geometry of the design disk (Figure 6) was configured using both finite difference and finite element techniques The geometry of the advanced standard disk is identical to that of the standard disk. Figure 7 shows a schematic of the standard and advanced standard disks.

The same thermal analysis was used to calculate transient and steady-state, radial and axial temperature gradients for the standard, advanced standard and design disks. P&WA's thermal analysis of a disk provides a complete and continuous temperature map throughout the entire flight cycle. This is required to determine steady state life limits associated with creep and

burst as well as transient conditions which affect low cycle fatigue limits. Steady state limits are examined at critical flight conditions, i.e., the worst combination of temperatures and rotor speeds. Transient temperatures are examined continuously over a flight cycle to provide a complete time temperature relationship for the entire disk

The thermal analysis is provided through the use of a three-dimensional transient finite element computer solution encompassing convection, conduction, and radiation. The environmental conditions influencing all external surfaces of the disk are defined as a function of time throughout the flight cycle and the metal temperatures along the disk surfaces and within selected interior nodes are generated by the computer deck. The boundary conditions are defined by correlations based on previous engine and rig experience.

Four major computer programs are used to produce the analysis described above. The following paragraphs describe each of these programs

- The first program is a generalized two-dimensional finite element break-up program which takes disk coordinates as input, and creates a fine mesh nodal break-up for thermal analysis. This deck is completely graphics interactive and makes use of digitizing equipment for generating coordinate input. The mesh fineness is variable throughout the part as accuracy requirements dictate. Disk three-dimensional effects must be input by hand

- The second program calculates all heat transfer coefficients and thermal boundary conditions required for thermal analysis throughout an entire engine flight cycle. Input consists of engine flowpath performance parameters, time response of boundary cooling air temperatures, and numerous types of heat transfer coefficient correlations. These heat transfer coefficient correlations are both analytical and experimental, and have been accumulated through years of research and through matching engine transient thermal data.

- The third program is a three-dimensional computer program which takes as input all information from the first two programs and yields all desired disk transient and steady state temperature profiles. This program calculates all conduction, convection, and radiation heat transfer by an implicit solution technique which incorporates a dynamic time step expander and contractor which assures that the transient time step is small enough to insure accuracy, but as large as possible to conserve computer time.

- The fourth program is a computer deck which reads thermal files created by the temperature calculation program discussed above and arranges the data for input into the stress decks for structural analysis.

Figure 8 shows the finite element thermal models of the advanced standard and design disks and Figure 9 shows the rim and bore averaged surface temperature profiles of the disks for the design flight cycle. A review of the thermal analysis of the standard disk was conducted and the corresponding temperature profile of the disk is also included in Figure 9 for comparison purposes. It is noted that the temperature distributions between the Waspaloy® standard disk and the Astroloy advanced standard disk are similar. This is because the geometry and the cooling scheme of the two disks are the same and the difference in thermal conductivity and specific heat properties of Waspaloy® and Astroloy are insignificant within the temperature range the disks operate The design disk temperature profile, however, shows a significant difference the rim and bore temperature profiles of the design disk, during engine ascent and descent in the flight cycle, never crossed each other as noted in the temperature profiles of the standard and advanced standard disks (Figure 9) The radial and axial temperature distributions are shown in Figure 10 for the standard and advanced standard disks and in Figure 11 for the design disk at pertinent points in the flight cycle. The elimination of the reverse temperature gradient (bore hotter than rim) during engine ascent and descent, and the reduction in the direct disk bore to rim temperature gradient (rim hotter than bore illustrated in Figure 10 and 11) are the results of the bore-entry-cooled, design disk concept

The stress analysis of the standard disk was reviewed, and the analysis of the advanced standard and design disks, as regards the determination of nominal disk stresses, was performed using an elastic-plastic disk stress analysis.

The elastic-plastic analysis used for general disk stress analysis and disk radial growth of all commercial compressor and turbine disks is based on a finite difference technique where the disk is modeled as a series of connected, concentric rings of variable ring width and thickness. The plastic capability is achieved by iteration from an initial elastic solution, bringing each ring to its proper location on the material stress-strain curve. The iteration procedure is generally convergent for practically all time points in the flight cycle history because of the constrained nature of disk bore plasticity. Stress analysis and growth data are generated for many, typically 100, time points within a flight cycle and include the effects of plasticity within the disk bore. Loading data for this disk program includes the previously computed thermal gradients and the inertial loads at the given rotational speed due to blade and attachment pull plus disk spacer, hub, sideplate, and seal loads Some of the loading data is externally supplied, the remainder is generated internally. The elastic-plastic analysis uses simple shell elements that can be used to compute radial disk loads due to seal appendages, the analysis generates rim loads from specified geometrical parameters.

The elastic-plastic stress analysis outputs the flight cycle time history of the local nominal stresses and strains, radial disk growth, disk burst margin, local values of stress concentrations, and LCF and fracture mechanics lifetime data The LCF and fracture mechanics analyses are described in Section 3 of this report. The stress concentration factors are derived by curve fit routines in the analysis for many classes of stress risers, the remainder are supplied as data from more refined elastic stress analysis described below

In the analysis of the advanced standard and design disks, the elastic-plastic analysis searched the design flight cycle for limiting stress points for the two disks and was consistent with the analysis performed on the standard disk. The stress analysis included effects of blade load, blade-to-disk attachment, thermal stresses, plasticity, acceleration and deceleration transients and other conditions that are considered in current disk design practice. The same analytical techniques were used in the analysis of the three disks where applicable. Figure 12 shows the nominal disk rim and bore stresses of the standard, advanced standard, and design disk. It is noted that the design disk rim has the least extensive stress cycling (stress fluctuation), within one flight cycle, of the three disks.

In the design disk, the centrifugal rim load on the disk is reacted by the bonded bore halves. Since the reactions are not in the same plane as the disk rim load, two couples (moment loads) are introduced in the bonded disk which cause the bore halves to roll toward each other inducing high axial compressive stresses in the disk radial vanes at the ID location. To reduce the local high axial compressive stresses, alternate radial vanes were extended to the disk bore radius as shown in Figure 6. Mixed body of revolution and plane stress finite element techniques were used in the determination of the axial vane stresses. The finite element analysis utilizes general quadrilateral plate or axisymmetric elements, assembled from constant strain triangles. In the analysis, the design disk structure was modeled using combined plate and axisymmetrical elements, the plate elements were used to model the disk lugs and radial vanes, the axisymmetrical elements were used to model the continuous axisymmetrical hoop material. Figure 13 shows a schematic of the finite element model of the design disk. The resulting axial stress distribution at the bond surface of the design disk is shown in Figure 14. The maximum bond tensile stress is 1.52×10^8 N/cm^2 (22 ksi) and the maximum bond compressive stress is -7.25×10^8 N/m^2 (-105.2 ksi) which is below the 0 2% yield strength of the material. Both of these stresses occur at 56 seconds into the flight cycle.

The same finite element analysis was used in the determination of stress concentration factors (SCF) at pertinent locations in the design disk, such as at the radial cooling air channel entrance and exit locations. Figures 15 and 16 show the finite element models of the design disk broach slot and cooling air channel cross-section, respectively, at the disk rim The finite element model of the cooling air channel cross-section (Figure 16) is typical of analytical models of the channel cross-section at the various disk radial locations such as at the disk web and bore. The pertinent SCF's, the limiting concentrated stresses and their corresponding locations in the standard, advanced standard and design disks are summarized in Table I. The limiting flight cycle time points associated with these stress occurrences are also included in the same table. These time points were the limiting flight cycle time points used in the crack initiation analysis.

Based on the thermal and stress analysis that had been conducted on the standard disk, creep was found not to be a limiting design consideration and this was also true for the advanced standard and design disks The advanced standard and design disks use the same blades and blade-to-disk attachments as in the existing standard disk. The disk attachments are subjected to the same centrifugal loads and, hence, the same attachment stresses are expected in all three disks. Figure 17 shows the attachment stresses for the three disks at the maximum engine take-off speed (11870 rpm)

TABLE I

LIMITING CONCENTRATED STRESS & FLIGHT CYCLE TIME POINT
SUMMARY OF STANDARD, ADVANCED STANDARD & DESIGN DISKS

Disk	Location: Radius cm	Location: Radius Inches	Remarks	Stress Concentration Factor	Limiting Stress: 10^8 N/m^2	Limiting Stress: ksi	Stress Type	Limiting Flight Cycle Time Point, Seconds
Standard Disk	21.6	8 51	Rim Cooling Air Exit Hole	3 45	10.4	151.9	Hoop	874.0
Advanced Standard Disk	21.6	8 51	Rim Cooling Air Exit Hole	3.45	10.3	149 8	Hoop	883.0
Design Disk	21 6	8.51	Rim Cooling Air Channel Exit	3.13	9.8	142.0	Hoop	7.5
Design Disk	17.8	7 0	Web Maximum Radial Stress Location	2 24	9.46	137 6	Hoop	300.25
Design Disk	9.2	3.60	Short Vane I. D	1.72	9 85	143.2	Hoop	56.0
Design Disk	6 0	2.35	Bore Cooling Air Channel Entrance	1.52	10.2	148 0	Hoop	225.25
				1.2	-8.75	-127.6	Axial	56 0

3.0 DISK FAILURE ANALYSIS

Low cycle fatigue and fracture mechanics theories were used in the failure analysis of the standard, advanced standard, and design disks. The overspeed capabilities of the three disks were also determined The total disk life was calculated based on the sum of the crack initiation and crack propagation periods for each of the three disks Further analysis of the design disk was conducted to increase its life. A fragment energy analysis was performed to calculate the total kinetic energies of potential disk fragments from the standard, advanced standard, and design disks.

3.1 CRACK INITIATION ANALYSIS

The crack initiation analysis for the three disks was based on the simplified JT8D-17 engine flight cycle (Figure 3) and on low cycle fatigue (LCF) theory P&WA's LCF life prediction system is an automated procedure which utilizes loading taken directly from the flight cycle history of the engine, elastro-plastic stress analysis utilizing the analysis tools described in Section 2.0, and the mechanical properties data base for the material system. LCF life is defined to be the generation of a .079 cm (1/32 inch) surface length crack from unflawed material based on a probability of one occurrence in one thousand disks.

The flight cycle history for an engine component such as the first stage turbine disk includes rotational speed and component temperature distribution. The nominal stress distribution is computed using the two-dimensional finite element and the elasto-plastic disk stress analysis programs described previously. Local values of stress concentration factors are then computed at each geometrical stress riser (e.g , blade attachment lug) using a two-dimensional finite element analysis.

For a given flight cycle, the nominal stress history at each stress concentration location is determined. The stress history for an engine flight cycle generally consists of a major stress cycle together with several minor stress cycles (a cycle is a complete reversal of the stress-strain values as shown in Figure 18). The strain range for the major and minor cycles are computed for each flight cycle by multiplying the nominal stress (strain) values by the computed stress (strain) concentration factor. The LCF life prediction analysis estimates the LCF life at each stress concentration location using an empirical function to determine the damage for the cycles defined by strain range and mean stress; the empirical function includes the effects of temperature, hold time, surface finish, and additional factors derived from extensive hardware experience. The cumulative effects of major and minor cycles are added using the standard linear cumulative damage rule (Miner's rule) Correlation of the LCF life prediction analysis results with engine-experience is good; furthermore, it is reasonably conservative as shown in Figure 19.

The LCF life summary of the three disks, Figure 20, shows that both the standard and advanced standard disks are LCF life limited at the disk rim cooling air hole exit location with 16,000 cycles and 18,000 cycles, respectively. The preliminary design disk is LCF life limited (23,000 cycles) at the disk bore cooling-air channel entrance location as well as at the disk sideplate snap location.

The overspeed capability, or burst margin, of the advanced standard and design disks was calculated using the same analytical procedure employed in the standard JT8D-17 first-stage high pressure turbine disk design Accurate means of predicting the burst speed of compressor and turbine disks have been developed through an extensive program which included the evaluation of the basic tensile properties (yield and ultimate strengths) of disk materials, the calculation of disk stresses, and the correlation of these stresses to the strength of the material through actual burst tests. It has been possible through actual whirl pit tests of approximately 300 disks to determine a correlation between the calculated average circumferential stress at burst and the ultimate strength of the material. Such a correlation has provided a consistent ability to predict the minimum burst speed of compressor and turbine disks. The burst strength of the disk has been related to the minimum ultimate strength of the material at the average disk temperatures. In all cases, minimum disk dimensions and maximum spacer and rim loads have been utilized and no consideration given to whatever restraining effects spacers and hubs might offer the disk. Burst margins, established by comparing disk burst speeds to the maximum, or redline, speed of the engine for the standard, advanced standard and preliminary design disks are 35.6%, 35.9% and 28.5% respectively, and they are all above the design minimum of 22%.

3.2 CRACK PROPAGATION ANALYSIS

The crack propagation analysis for the standard, advanced standard, and design disks was based on assumed orientation, size, shape, and location of initial flaws for three critical locations, shown in Figure 21, in each of the three disks using fracture mechanics theory.

The fracture mechanics analysis for predicting crack growth under flight cycle loading is broken into two classes of problems; growth of a subsurface crack from an inherent material defect and, continued growth of a surface crack initiated by LCF loading of unflawed material as described in Section 3.1. In both cases of crack growth, the empirical elastic fracture mechanics correlation of the crack growth rate (da/dn) and the crack tip stress intensity factor for each stress cycle (ΔK) is numerically integrated to determine crack size as a function of cycle numbers. Use of the "influence function" method (ref. 2) in the fracture mechanics analysis for evaluating crack tip stress intensity fields fully accounts for local stress variation at the crack due to geometry changes as the crack grows. The analysis assumes the magnitude and distribution of the forces and stresses in the gross structure are not influenced by the crack itself.

The subsurface crack growth analysis is based on the inherent material defect size, the local nominal stress cycle and mean stress level, the local temperature, and the necessary material parameters. These material parameters include the threshold value of stress intensity factor, the fracture toughness, and the empirical values of crack growth rate as a function of temperature and the ratio of maximum to minimum stress for a stress cycle. The subsurface

(2) Cruse, T. A. and Besuner, P. M., "Residual Life Prediction for Surface Cracks in Complex Structural Details," Journal of Aircraft, Vol 12, No 4, April, 1975, pp. 369-375.

crack stress intensity factor is computed using the theoretical results for a buried flaw, circular in shape, and oriented transverse to the maximum normal stress component. The subsurface crack size is given a statistical variation which may be truncated for cracks larger than a specified minimum inspection level; the material parameters are also fit to statistical functions to account for real material variability. The fracture mechanics life (cycles to grow a crack to the critical crack size for the local stress cycle) is obtained using an analysis which combines the statistics of flaw size, material properties, and the actual load cycle. The resulting life is based on the probability of one failure in ten thousand disks.

The major difference between the subsurface crack and surface crack problems is the need to account for the effects of both crack size and shape together with the stress gradients inherent to notched geometries. Reference 2 describes the techniques used for simulating surface crack growth including these complexities, numerical modeling of surface cracks is accomplished using the boundary-integral equation technique.

The boundary-integral equation method of stress analysis differs significantly from finite element stress analysis. A set of constraint equations relating boundary tractions to boundary displacements is solved numerically; the technique requires that only the boundary of the geometry be modeled. Thus the numerical problem of modeling the interior, as done by the finite element method, is avoided, resulting in better resolution of high stress/strain gradients; further, problem size and computer run time are significantly reduced relative to comparable finite element results.

The types of flaws considered in this study can be divided into three categories

- Surface flaws located in the LCF initiation sites at the cooling hole exit of the standard and advanced standard disks and at the cooling channel entrance to the design disk (Figure 22)

- Manufacturing flaws buried in the bores of all three disks.

- Manufacturing flaws in the disk webs including buried flaws in the web of the standard and advanced standard disks, and a flaw at the TLP® bond line of the design disk, propagating from a sharp corner created by a misalignment of the two disk halves during fabrication (Figure 23).

The crack growth rates used in the fracture mechanics life prediction analysis of the three disks are based on 700°K (800°F) crack growth data of conventionally forged Waspaloy® and Astroloy. The 700°K (800°F) crack growth data was used in the analysis because of limited data available for temperatures between room temperature and 700°K (800°F) Use of 700°K (800°F) data is conservative since 700°K (800°F) crack growth rates tend to be greater than room temperature rates for these materials, and the temperature rises above this level only at time points in the flight cycle having low stress (Table II).

The stresses and temperatures used in the crack propagation analysis of the three disks were obtained from the results of the flight cycle analysis shown in Figures 9 and 12. The critical time points from the flight cycle analysis and the corresponding nominal stresses and temperatures are summarized in Table II. At the time points of maximum stress (the points used

in the crack growth analyses), the temperatures are all below 700°K (800°F), which is the baseline temperature used for the generation of the crack growth rate data Temperatures exceeding 700°K (800°F) are seen only in conjunction with stresses considerably less than the maximum stress value. Local stress profiles and stress concentration factors from finite difference and finite element analysis were included in the crack propagation analyses of the LCF-initiated cracks in the three disks.

In the standard and advanced standard disks, a substantial subcycle in the hoop stress occurred at the rim (Figure 12). In the fracture mechanics analysis, this subcycle was treated as being completely equivalent to the major cycle because the value of maximum stress of the minor cycle is within 10% of maximum stress in the major cycle, and the difference in temperature at the two points could not be accounted for analytically since only one temperature, 700°K (800°F), crack growth data was used. Furthermore, testing on nickel materials shows no significant dwell effects at temperatures considered Therefore, the crack propagation lives quoted for the cooling channel exit locations for the standard and advanced standard disks account for two load cycles per flight.

The crack initiation life as calculated by P&WA's LCF life prediction system is defined to be the generation of a 0.079 cm (1/32 inch) surface crack. This surface flaw was assumed to be semi-elliptical in shape and the orientation of the flaw was such that the plane containing the crack front was normal to the local stress field. The growth of this surface flaw in the fracture mechanics analysis was assumed to propagate in an infinite width structure. This assumption is valid for a surface flaw depth less than or equal to three-fourths of the structural finite width, based on P&WA's in-house experience. The initial ratio of crack depth to crack surface length (a/c) for the 0.079 cm (1/32 inch) surface crack was obtained by analytically "growing" to the 0.079 cm (1/32 inch) size from a 0.01 cm (0.004 inch) semi-circular crack. Local stress profiles determine the aspect ratio. The initial ratio of crack depth to crack surface length (a/c) is 0.48 for the surface flaw at the cooling hole exit location of the standard and advanced standard disks (Figure 22). The crack propagation lives of this flaw in the standard and advanced standard disks are 2900 and 1150 cycles, respectively; and the corresponding critical flaw size for the two disks is shown in Figure 24. The initial crack depth to crack length aspect ratio of the preliminary design disk is 0.44 (Figure 22) and the critical flaw size shown in Figure 25, is limited at 4900 cycles The critical flaw depths for all three disks are within the size limits of the analytical assumptions noted above.

In the manufacturing of the standard, advanced standard, and design disks, the disks undergo a forging process prior to machining. Because of the forging process, intrinsic material flaws in the disk are assumed to become preferentially oriented parallel to the disk forging flow or normal to the sonic inspection direction. Therefore, the assumed subsurface material flaws (Figure 21) of the three disks are based on a sonically detectable, penny-shaped, flat-bottomed buried flaw of 0.119 cm (0.047 inch) diameter. The crack propagation life prediction system then relates the sonic inspection and material data to a corresponding penny-shaped, buried, flat-bottomed hole normal to the maximum stress direction to determine the crack propagation life of the sonically identified 0.119 cm (0.047 inch) diameter flaw.

The buried manufacturing flaws in the bores of the standard, advanced standard, and design disks were analyzed using the maximum hoop stress in the individual disk bore. The calcula-

TABLE II

CRITICAL TIME POINTS IN FLIGHT CYCLE

Location			Time Sec.	Temperature °K (°F)	Stress 10^8 N/m^2 (ksi)	Direction
I.	Design Disk					
	1.	Cooling channel entrance	a) 300 25	661 (730)	6.73 (97.6)	Hoop
			b) 150.25	670 (746)	6.59 (95.6)	Hoop
	2	TLP® bond	a) 56 00	666 (740)	1 52 (22.0)	Axial
			b) 150.25	700 (800)	<1.52 (<22 0)	Axial
	3	Bore	a) 300 25	661 (730)	6.73 (97.6)	Hoop
			b) 150 25	670 (746)	6 59 (95 6)	Hoop
II.	Advanced Standard Disk					
	1.	Cooling channel exit	a) 1528 00	522 (480)	3.06 (44 4)	Hoop
			b) 75 25	755 (900)	0.38 (5.5)	Hoop
			c) 7.50	461 (370)	2 82 (40 9)	Hoop
	2	Web	a) 70 00	650 (710)	5.76 (83.6)	Radial
			b) 300 25	716 (830)	4 61 (66.9)	Radial
	3	Bore	a) 430.00	695 (792)	6 18 (89 7)	Hoop
			b) 70 00	708 (814)	3.77 (54.7)	Hoop
III	Standard Disk					
	1	Cooling channel	a) 1519.75	528 (490)	3 10 (44 9)	Hoop
			b) 73 00	755 (900)	0 24 (3 5)	Hoop
			c) 7 50	461 (370)	2 90 (42 0)	Hoop
	2.	Web	a) 70.00	650 (710)	5 86 (85.0)	Radial
			b) 298.00	716 (830)	4 71 (68.3)	Radial
	3.	Bore	a) 430 00	695 (792)	6 21 (90 0)	Hoop
			b) 70.00	710 (818)	3 59 (52.0)	Hoop

a) Point of maximum stress
b) Point of maximum temperature
c) Stress subcycle (Figure 12)

ted crack growth lives for the standard, advanced standards, and design disks are 65,000, 39,000, and 26,000 cycles, respectively, and the corresponding critical flaw diameters are 2.46, 2 46, and 2 11 cm (0.97, 0.97, and 0.83 inches), respectively.

The manufacturing flaws in the webs of the standard and advanced standard disks, under maximum radial stress, were calculated to be 97,000 cycles and 59,000 cycles, respectively. The corresponding critical flaw diameter for both disks at this location is 1 80 cm (0.71 inches) before rapid fracture.

Due to manufacturing tolerance buildup in the design disk, there can be a misalignment at the TLP® bond surface between the cooling channel vanes of the two disk halves creating a sharp corner at the bond line (Figure 23). It was assumed that an initial crack would occur upon the first load cycle because of the high local stress intensity at the sharp corner although the normal tensile stress in the bond is low, 1.52×10^8 N/m^2 (22 ksi). This crack at the TLP® bond line (Figure 23) of the design disk was analyzed as a two-dimensional crack The geometry is such that the problem does not have an exact solution, therefore, a graph of stress intensity factor (ΔK) vs. crack length was determined, Figure 26 This analysis shows that the value of ΔK is above the threshold value only for very short crack lengths. For only slightly longer crack lengths, the value of ΔK drops well below threshold. This means that the crack cannot grow, since $\Delta K_{THRESHOLD}$ is defined as that value of ΔK below which no growth can take place. Therefore, infinite life was found for this location.

3.3 DISK LIFE IMPROVEMENT

Results of the crack initiation analysis on the design disk indicated that the limiting LCF locations were at the disk bore cooling-air channel entrance and at the disk sideplate snap, and the life was 23,000 cycles at each location. In order to improve the LCF life of the design disk, design modifications were made and a re-analysis of the disk was performed In the re-analysis, the original design disk temperature distribution was used because the small temperature variation resulting from the design changes would have an insignificant effect on the disk stresses.

To improve the life of the disk bore, both hoop and axial stresses had to be reduced. A reduction in hoop stress was accomplished by increasing the live bore thickness from 6.35 to 7.19 cm (2.5 to 2.83 inches) (13% increase). However, this increase had an adverse effect on the axial stress at the cooling channel vane ID. Under a centrifugal field, the two bore halves have a tendency to roll toward each other because of the induced moment load in the disk caused by the offset between the centrifugal rim load on the disk and reactions of the bore halves. The rolling movement was aggravated by the bore thickness increase and induced a higher axial stress at the vane ID. To relieve the high compressive local stress, the minimum radial vane thickness was increased from 0.178 to 0.203 cm (0.070 to 0.080 inches). This was accomplished by specifying tighter tolerances on the cooling air channel dimensions at the disk bore. The improved disk bore cooling-air channel entrance LCF life is 30,000 cycles.

The weight of the original design disk was 1.36 kg (3 lbs.) lighter than the standard B/M disk. With a 13% increase in bore material, the weight of the improved design disk equals that of the standard B/M disk. This design change would not yield significant, if any, life improvement for the standard and the advanced standard disks. A review of the temperature versus flight time profiles of the standard, advanced standard, and design disks at their respective bores and rims, shown in Figure 9, indicated that the rim and bore temperature profiles of the design disk, during engine descent in the flight cycle, never crossed each other as did the temperature profiles of the standard and advanced standard disks. The elimination of the reverse temperature gradient (bore hotter than rim) during flight descent is the reason that in the design disk the addition of bore material to the disk reduces the circumferential bore stresses while not aggravating the rim stresses of the disk. In the standard and advanced standard disks, the addition of bore material increases the disk bore mass which increases the existing reverse temperature gradients in the two disks by further delaying the thermal response of the disk bore with respect to the rim during engine flight descent. This increased reverse temperature gradient causes the hotter bore to induce more strain on the cooler rim resulting in an increased circumferential stress field at the rim where the standard and advanced standard disks were already LCF limited.

To further improve the LCF life of the design disk sideplate snap, the original sideplate snap was redesigned to allow for a smoother local stress flow and hence reduced stress concentration and improved LCF life. The critical stress in the sideplate snap is 9.20×10^8 N/m^2 (133.3 ksi). The limiting LCF crack initiation life for the redesigned sideplate snap configuration is 33,000 cycles, a 43% improvement over the original design life. Figure 27 shows a drawing of the improved design disk. A summary of the limiting LCF crack initiation lives of the disk before and after the design change is shown in Table III. The burst margin in the improved design disk is 33%. Figure 28 shows the LCF crack initiation life summary of the standard, advanced standard and improved design disks.

The crack propagation analysis for the improved design disk was done in a manner paralleling that discussed in the previous section for the original design disk. Table IV compares the life predictions obtained for the improved design disk with those previously calculated for the original design disk. At the cooling channel entrance location, the crack propagation life of the improved design disk is 6,500 cycles which is 32% greater than the original design. Both disks show the same crack propagation life ($> 10^5$ cycles) at the TLP® bond line. Figure 29 shows the critical crack size of the surface flaw at the cooling channel entrance location of the improved design disk. Figure 30 shows the crack propagation life summary of the standard, advanced standard and improved design disks.

The improvement in life of the initially flawed improved design disk over the initially flawed standard and advanced standard disks is 124% and 465%, respectively, obtained by comparing the number of cycles to failure during the crack propagation period (Table V). The improvement in life of the initially unflawed design disk over the initially unflawed standard and advanced standard disks (93% and 90%, respectively) was obtained by comparing the totals of the number of cycles to crack initiation and the number of cycles during the crack propagation period (Table VI). A normalized weight comparison between the standard, advanced standard, and improved design disk is also included in Table VI.

TABLE III

LCF LIFE SUMMARY OF THE STANDARD, ADVANCED STANDARD, DESIGN AND IMPROVED DESIGN DISKS

Disk Identification	Disk Location	LCF Crack Initiation Life Cycles	
		Original Design	Improved Design
Standard Disk	Rim Cooling Air Hole Exit	16,000	–
Advanced Standard Disk	Rim Cooling Air Hole Exit	18,000	–
Design-Disk	Rim Cooling Air Channel Exit	30,000	35,000
Design Disk	Bore Cooling Air Channel Entrance	23,000	30,000
Design Disk	Sideplate Snap	23,000	33,000

TABLE IV

SUMMARY OF FRACTURE MECHANICS LIFE PREDICTIONS

		No. of Cycles	
		Original Design	Improved Design
1)	Surface Flaws at LCF Initiation Sites		
	a) Design disk cooling channel entrance	4,900	6,500
	b) Advanced standard disk cooling channel exit	1,150	–
	c) Standard disk cooling channel exit	2,900	–
2)	Manufacturing Flaws at Disk Webs		
	a) Design disk TLP® bond line	$>10^5$	$>10^5$
	b) Advanced standard disk web	59,000	–
	c) Standard disk web	97,000	–
3)	Manufacturing Flaws at Disk Bores		
	a) Design disk bore	26,000	37,000
	b) Advanced standard disk bore	39,000	–
	c) Standard disk bore	65,000	–

TABLE V

CRACK PROPAGATION LIFE IMPROVEMENT OF DESIGN DISK

Disk Identification	Crack Propagation Life (Cycles)	Life Improvement
Improved Design Disk	6,500	465% Over Advanced Standard Disk 124% Over Standard Disk
Advanced Standard Disk	1,150	
Standard Disk	2,900	

TABLE VI

TOTAL LIFE IMPROVEMENT OF DESIGN DISK

Disk Identification	Crack Initiation Life (Cycles)	Crack Propagation Life (Cycles)	Total Life (Cycles)	Life Improvement	Percent Weight
Improved Design Disk	30,000	6,500	36,500	90% Over Advanced Standard Disk 93% Over Standard Disk	100
Advanced Standard Disk	18,000	1,150	19,150	1.3% Over Standard Disk	96
Standard Disk	16,000	2,900	18,900	Base Line	100

3.4 FRAGMENT ENERGY ANALYSIS

Based on P&WA's burst experience, the failure patterns shown in Figures 31 and 32 are representative of how the three disks may fail due to crack progression from an LCF initiated flaw or from a buried material flaw. The fragment patterns, used for the fragment energy calculations, include three fragment patterns (size and number of fragments) for each of the three cracks analyzed in the standard, advanced standard, and design disks (a total of 27 fragment patterns).

P&WA's experience would not indicate any significant difference in burst patterns between the standard (Waspaloy®) and the advanced standard (Astroloy) disks. Also, P&WA's experience would not predict a significantly different fracture pattern for the design disk except that during the actual breakup, the two halves may separate and fracture into two different failure patterns.

The basic fracture mechanism for each of the assumed flaws (Figure 21) in each of the three disks is similar. A crack (or flaw) will progress with the principal stress field (tangential or radial) to a critical size when the disk will experience rapid fracture. During the course of crack growth, a crack can change direction, branch out into two or more cracks, induce other cracks or progress in one direction until it splits the disk, subject to the load redistribution in the damaged disk As a crack progresses, the centrifugal loads in the disk will cause the fracture surfaces to separate, transferring the load away from the failure origin. The transferring of the load away from the initial crack will cause cracks to form in other high stress locations due to tensile overload Significant progression of two or more of these cracks simultaneously will alter the stress fields in the disk in such a way that the actual failure pattern encompasses two or more fragments Figure 31 shows three possible disk fragment patterns which can result from a surface flaw at an LCF initiation site and the three possible disk fragment patterns which can result from a buried material flaw in the disk web and in the disk bore in the standard and advanced standard disks

The three major locations in the design disk where crack growth and eventual disk fragmentation could occur were also considered. Growth of a radial crack along the bond line due to manufacturing misalignments may lead to separation of a single vane of the design disk This separation is not critical to engine operation or the engine overspeed burst margin because of the great redundancy of the vane load paths and the fact that the bond surfaces are lowly stressed. Thus, the effect of redistribution and unsymmetry of load due to vane debonding is minimal and was not considered. Standard routine inspection of the disk is expected to locate such vane "debond" cracks. For these reasons, vane "debond" cracking is in a crack tolerant mode and no subsequent disk fragmentation can originate from this mode of cracking. However, these debond cracks can influence the fragment patterns and sizes of an LCF initiated bore crack or a buried material flaw initiated crack by allowing fractured disk fragments to separate at the bond line. Figure 32 shows the possible fragment patterns which can result from the influence of this manufacturing flaw.

The two other key sites of fatigue crack growth in the design disk are the crack growth in the bore associated with the growth of a buried material flaw and a surface flaw at the cooling-air entrance channel. In the presence of the much higher nominal disk hoop stresses of the bore, both modes of disk crack growth will tend to be critical for the load carrying capability of the disk as they will grow transverse to the disk hoop stress and are not likely to stop growing prior to reaching instability.

The design disk concept was assumed to have the capability of restricting these two modes of crack growth to one-half of the design disk. This restriction results from the presence of the radial cooling channels, as crack growth is expected to occur between the channel and the disk free surface. The potential to isolate crack growth to one-half of the design disk differs significantly from standard disk design where crack growth can fail the entire disk load carrying capability by fracture of the disk cross-section. The fragmentation of a portion of a design disk half, however, can effect the integrity of the adjacent disk half by overloading the disk lugs common to both and tearing them off with the fractured disk fragment. Possible design disk fragment patterns which can result from the LCF initiated bore crack and the buried material flaw in the disk bore are also shown in Figure 32

Fragment energy is defined as the total kinetic energy of a disk fragment (including the attached blades and side plates) upon fragmentation of the disk. The fragment energies of the disk fragments for the standard, the advanced standard, and the improved design disks were computed and are included in Figures 31 and 32. The standard disk made of Waspaloy, and the advanced standard disk, made of Astroloy, have the same disk geometry and disk fragment patterns The small difference in fragment energy between the two disks is due to the difference in densities between the two disk materials. The improved design disk, made of Astroloy, is geometrically different from the standard and advanced standard disks. The improved design disk, characterized by radial bore-to-rim cooling channels machined in two disk halves which are transient liquid phase bonded together, was assumed to result in the confinement of fragmentation to one-half of the disk and thus results in smaller fragments and hence, lower fragment energy as compared to the standard and advanced standard disk fragments, as illustrated in Table VII.

TABLE VII

FRAGMENT ENERGY COMPARISON BETWEEN STANDARD, ADVANCED STANDARD AND IMPROVED DESIGN DISKS

Fragment		Available Kinetics Energy, Joules (in-lb) @ 11870 rpm		
Pattern	Type*	Standard Disk	Advanced Standard Disk	Improved Design Disk
27 Blades and Disk Lugs; Sideplates and 120° Disk Segment	B	679,000 (6,010,000)	654,000 (5,780,000)	–
8 Blades and Disk Lugs; Sideplates and Disk Fragment Spanning 30° Circumferentially and above 17.8 cm (7.0 in) Radius	E	78,000 (690,000)	75,000 (665,000)	–
27 Blades and Disk Lugs; Sideplates and 120° Segment of Rear Disk Half	B	–	–	513,000 (4,540,000)
8 Blades and Disk Lugs; Sideplates and Segment of Rear Disk Half Spanning 30° Circumferentially and Avove 17.8 cm (7.0 in) Radius	E	–	–	72,000 (633,000)

*Reference Figures 31 and 32

CONCLUDING REMARKS

In the design of an increased reliability high pressure turbine disk, P&WA's study emphasized improving reliability by increasing cycle life of the disk without increasing the disk weight and without loss of engine performance. The improved design disk resulting from this study, a bore-entry-cooled bonded disk, could potentially replace the Bill-of-Material first-stage high pressure turbine disk in the JT8D-17 engine. This improved design disk has an LCF crack initiation life 87% and 67% greater than the standard and advanced standard disks, respectively Relative to the standard and advanced standard disks, the increase in crack propagation life for the initially flawed improved design disk is 124% and 465%, respectively. The overspeed capability, or burst margin, of the improved design disk is 33%, which is 50% above the design minimum. The improved design disk made of Astroloy weighs the same as the Waspaloy® standard disk. Based on the assumed disk fragments for the three disks (standard, advanced standard and improved design disks), the improved design disk has the smallest disk fragments and hence the lowest fragment energy. These analytical results indicate that the bore-entry-cooled turbine disk concept has the potential for significant improvements in turbine disk life in advanced engine designs. Therefore, it is recommended that improved design disks be fabricated and evaluated in fatigue and overspeed tests to verify the analytical results determined in the study

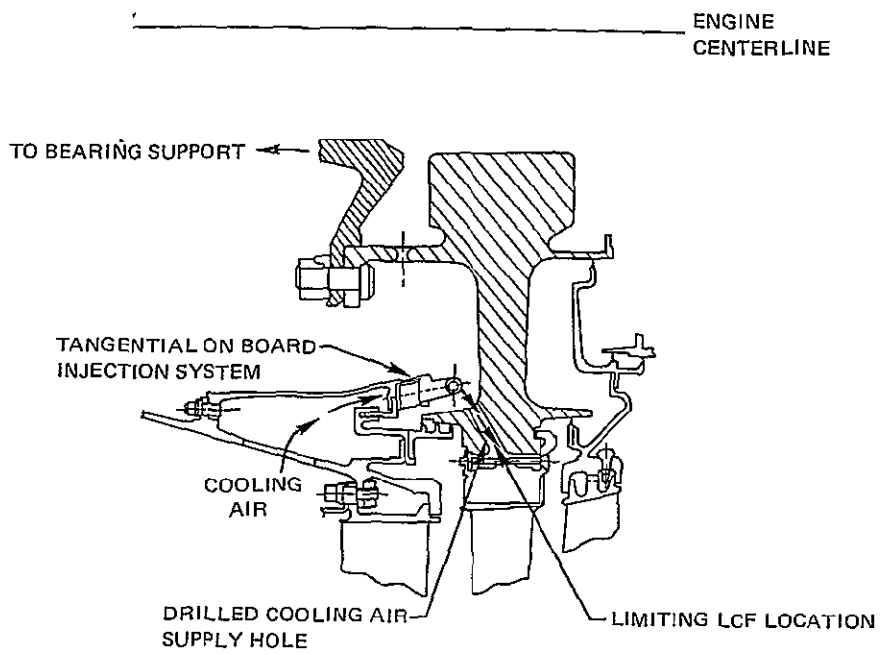

Figure 1 JT8D-17 High Pressure Turbine Disk Cross-Section

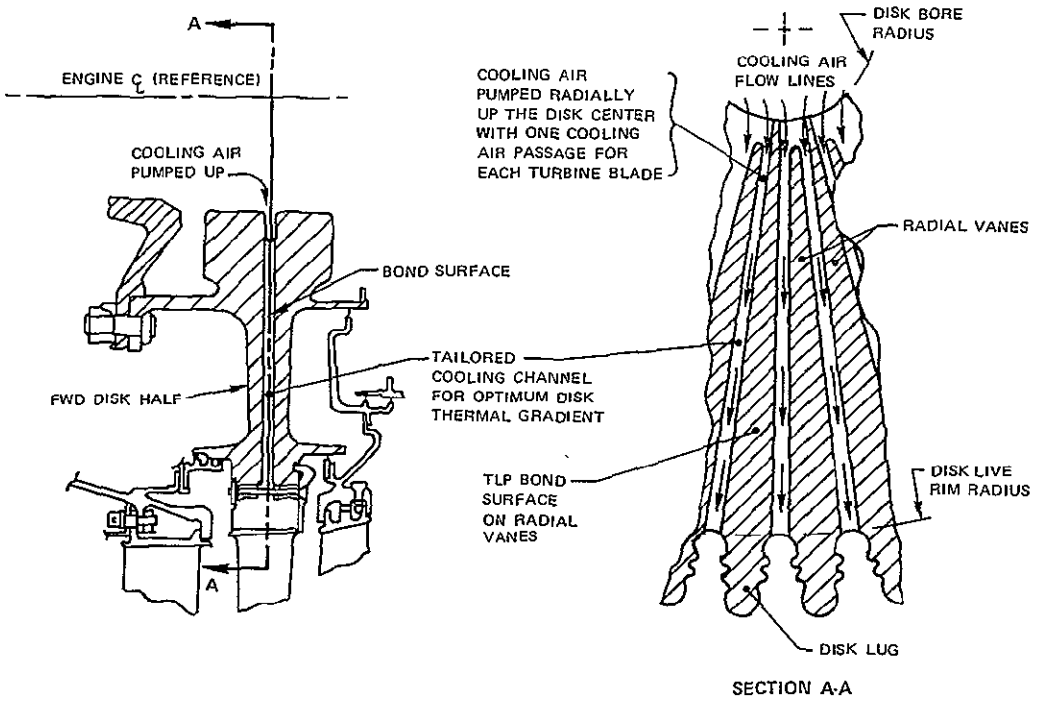

Figure 2 Bonded Design Disk Cross-Section

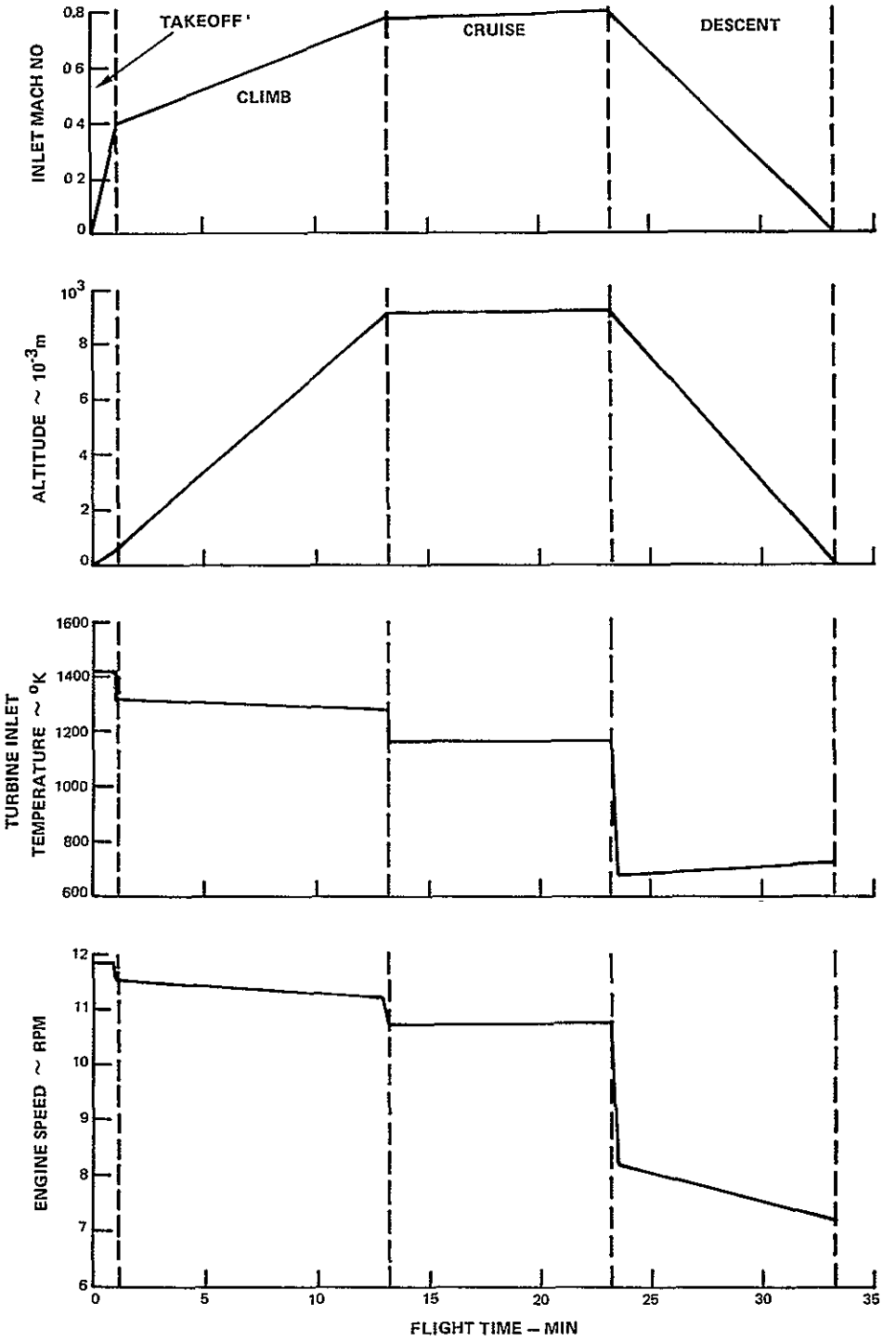

Figure 3 JT8D-17 Simplified Engine Flight Cycle

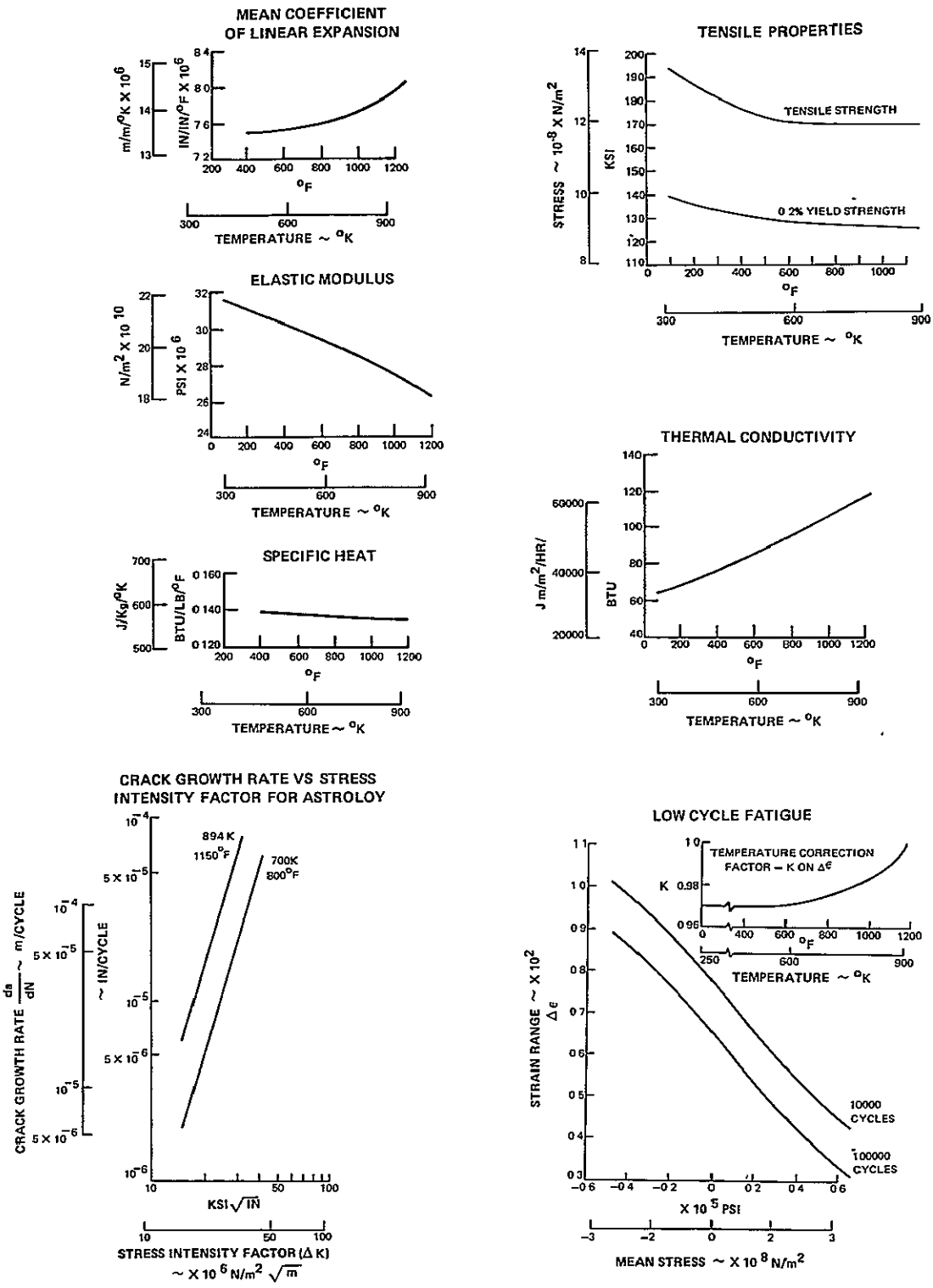

Figure 4 Design Properties for Astroloy

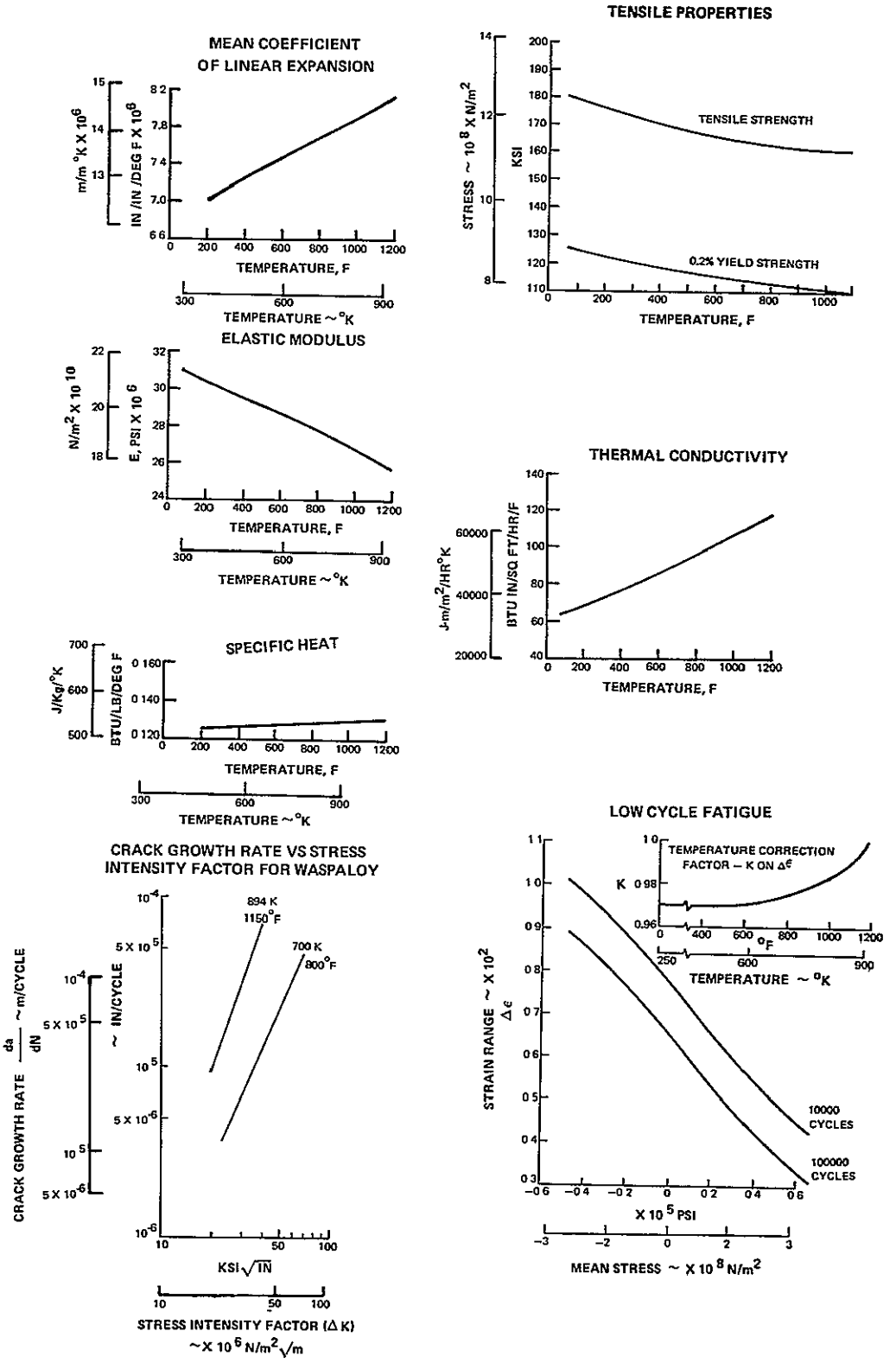

Figure 5 Design Properties of Waspaloy®

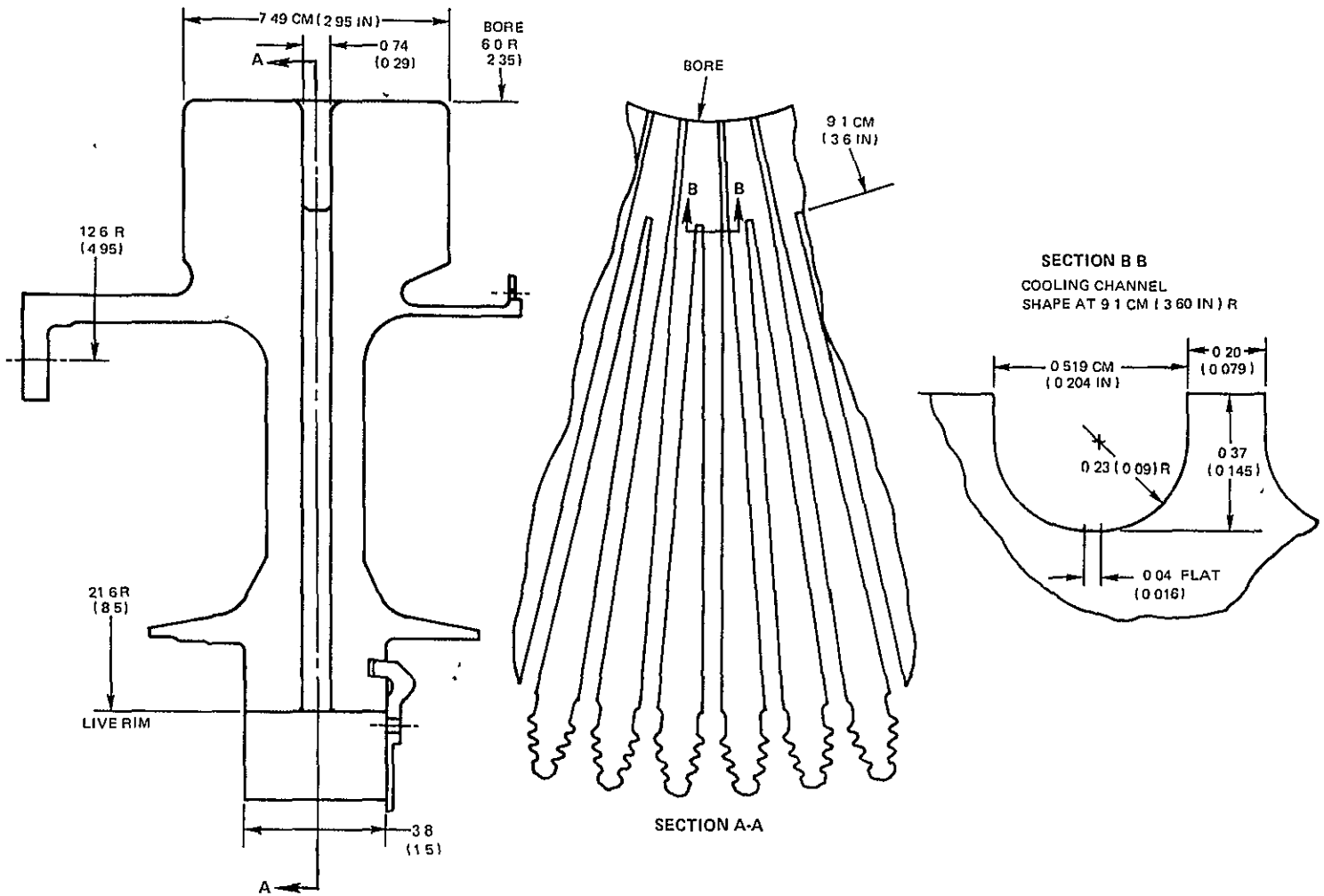

Figure 6 Schematic of Bonded Disk With Radial Cooling Air Flow Passages

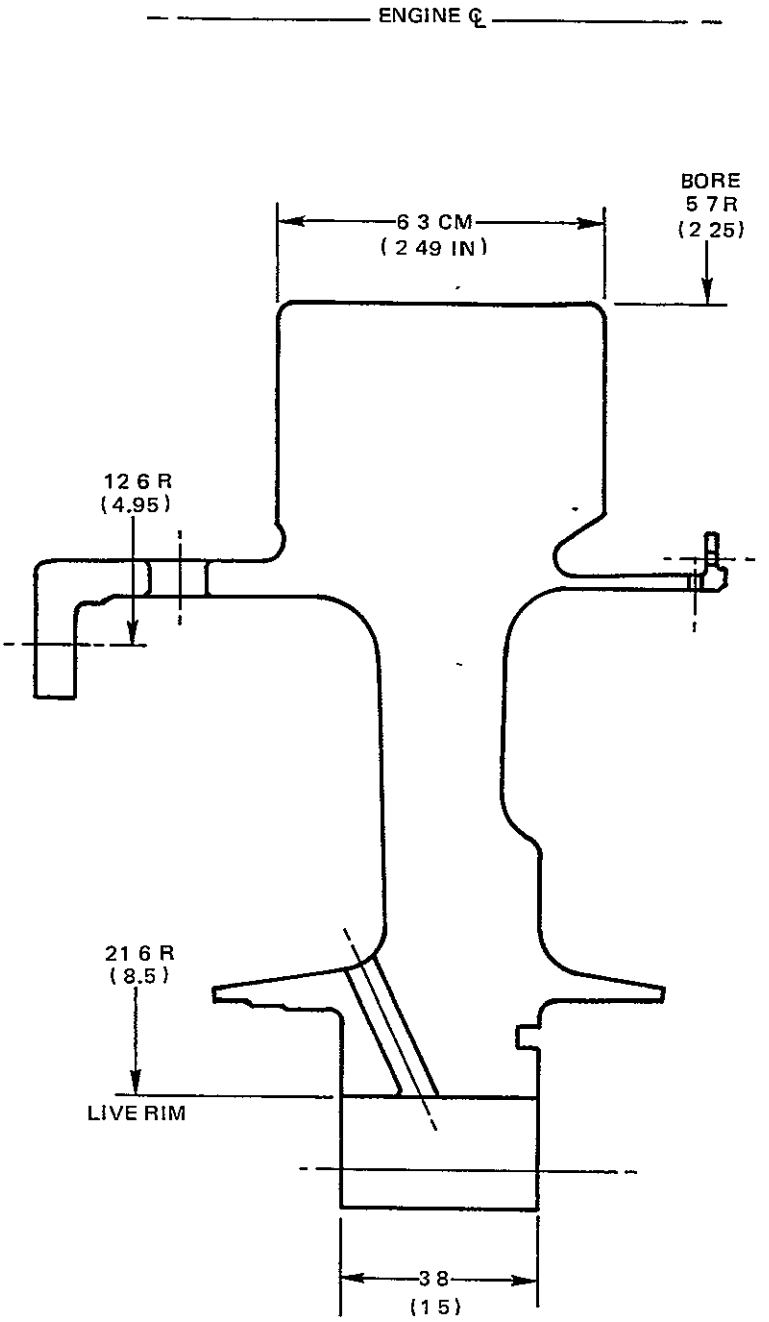

Figure 7 Schematic of Standard and Advanced Standard Disk

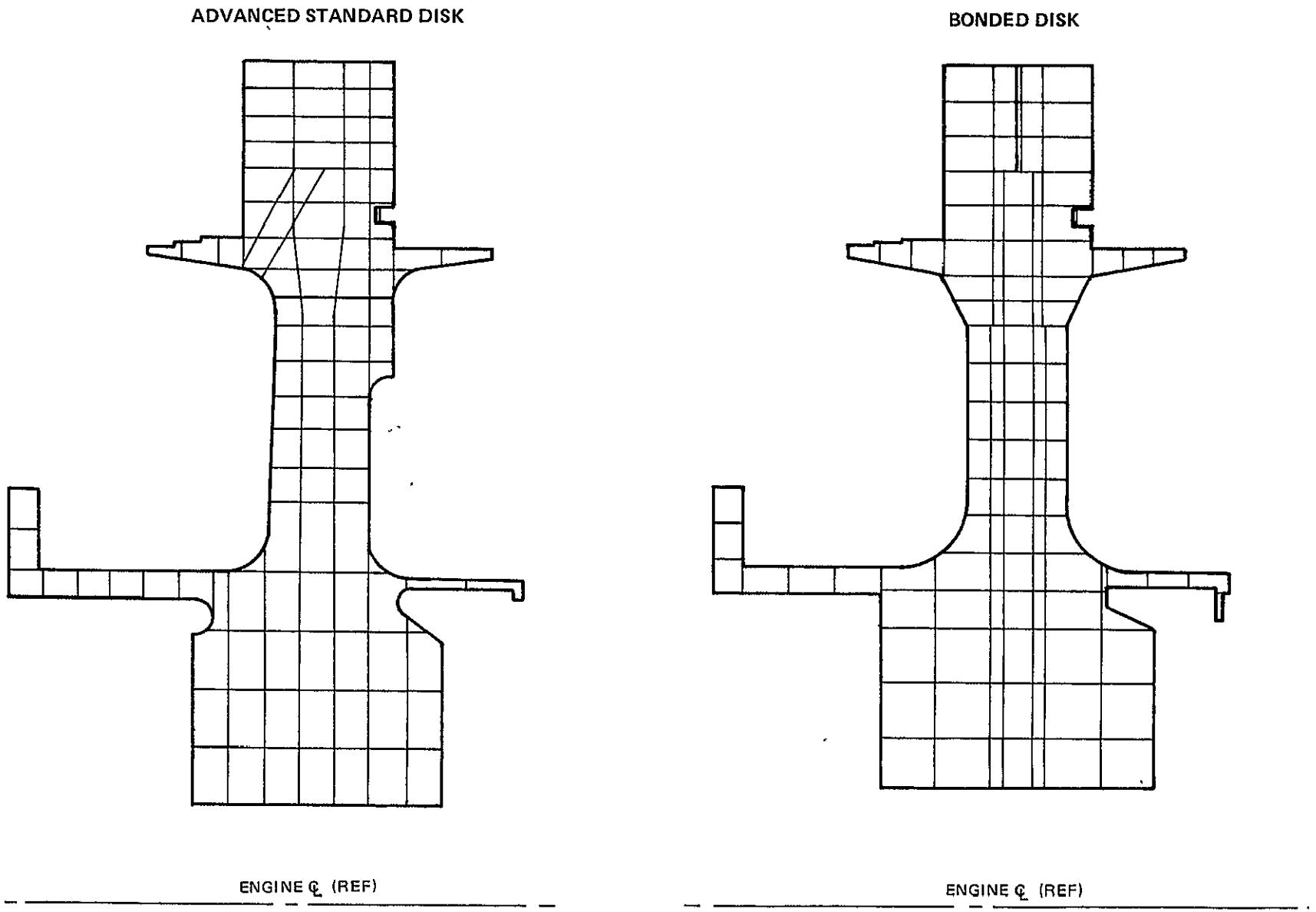

Figure 8 Finite Element Disk Thermal Models

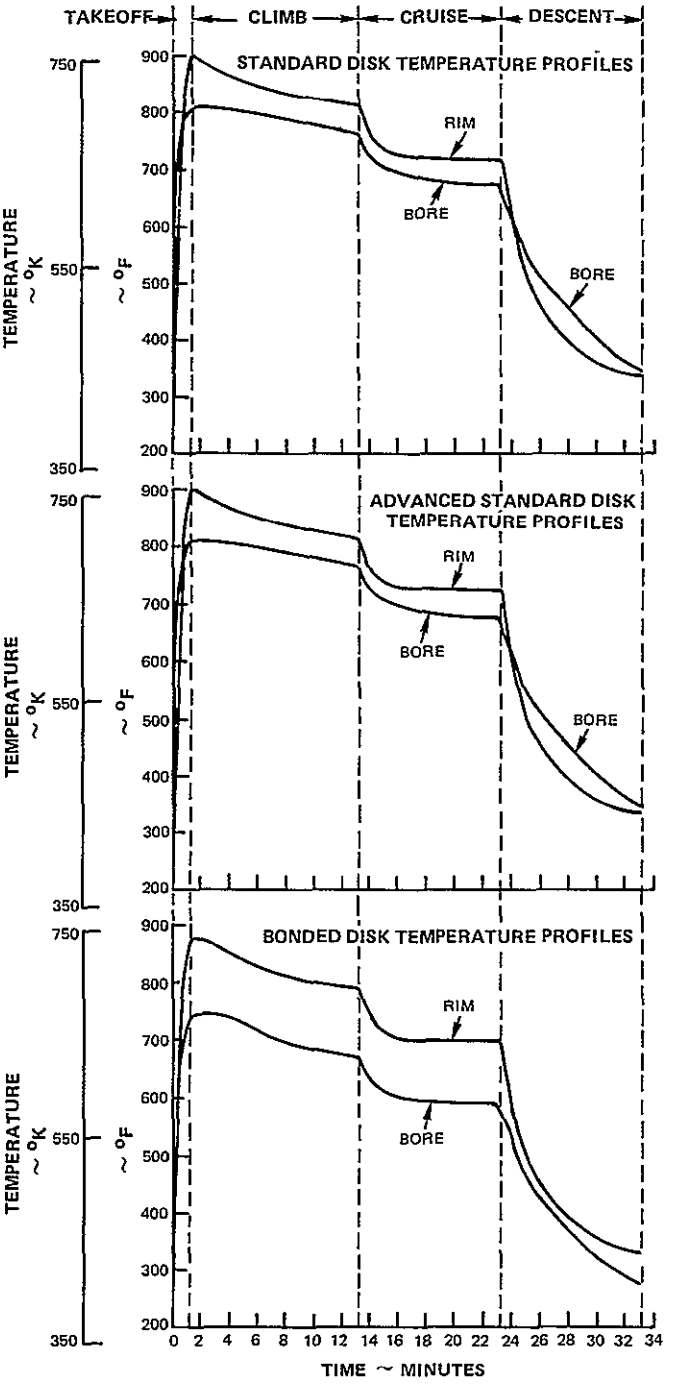

Figure 9 Disk Rim and Bore Averaged Surface Temperatures vs Flight Time

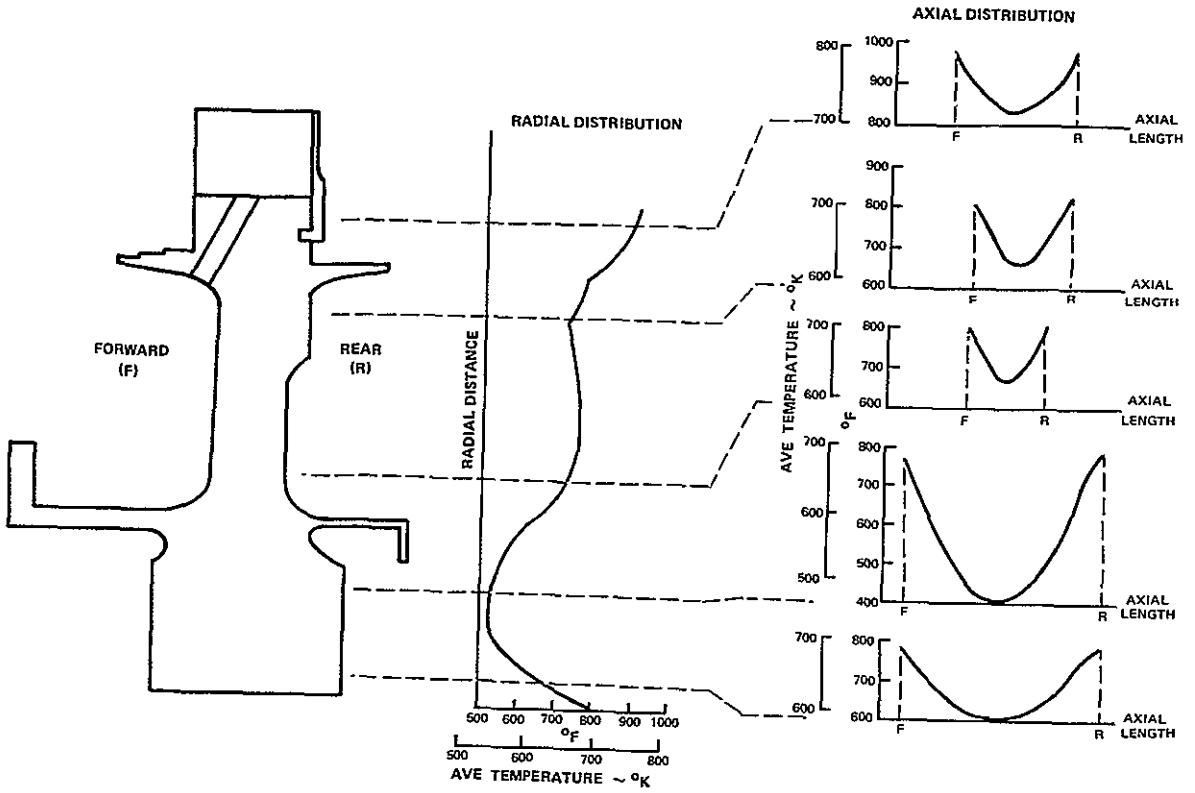

b. AT 790 SECS
(END OF CLIMB)

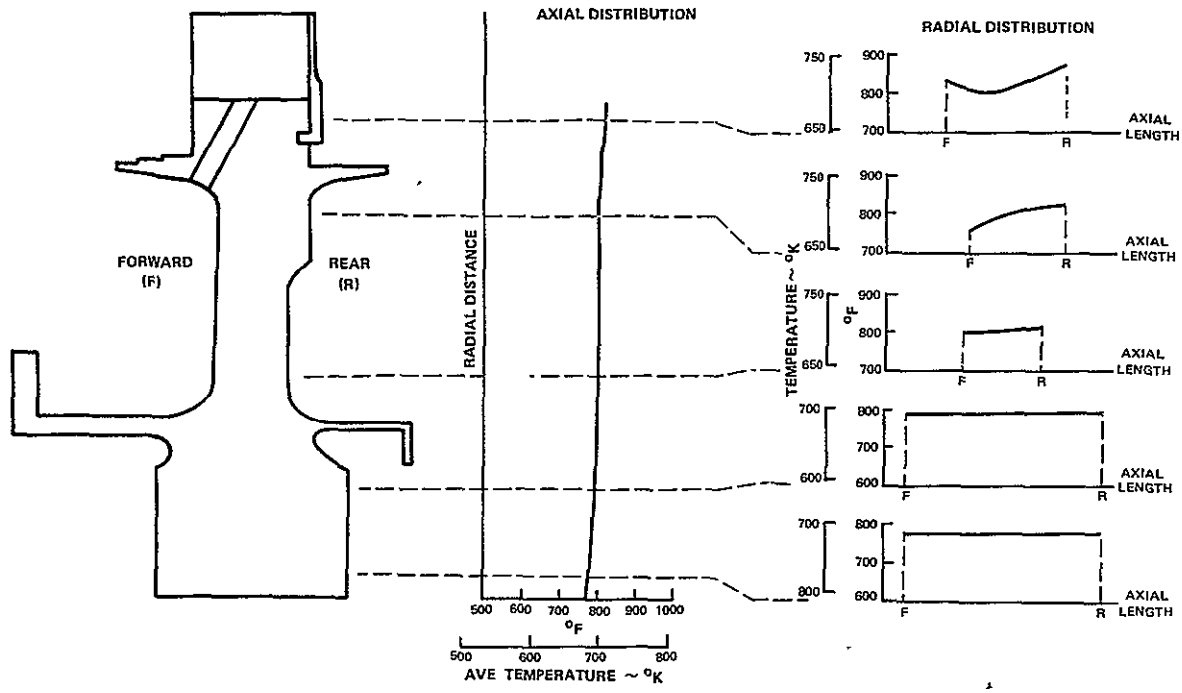

Figure 10 *Radial and Axial Temperature Distribution in Standard and Advanced Standard Disks at Pertinent Points in the Flight Cycle*

c. AT 1390 SECS
(END OF CRUISE)

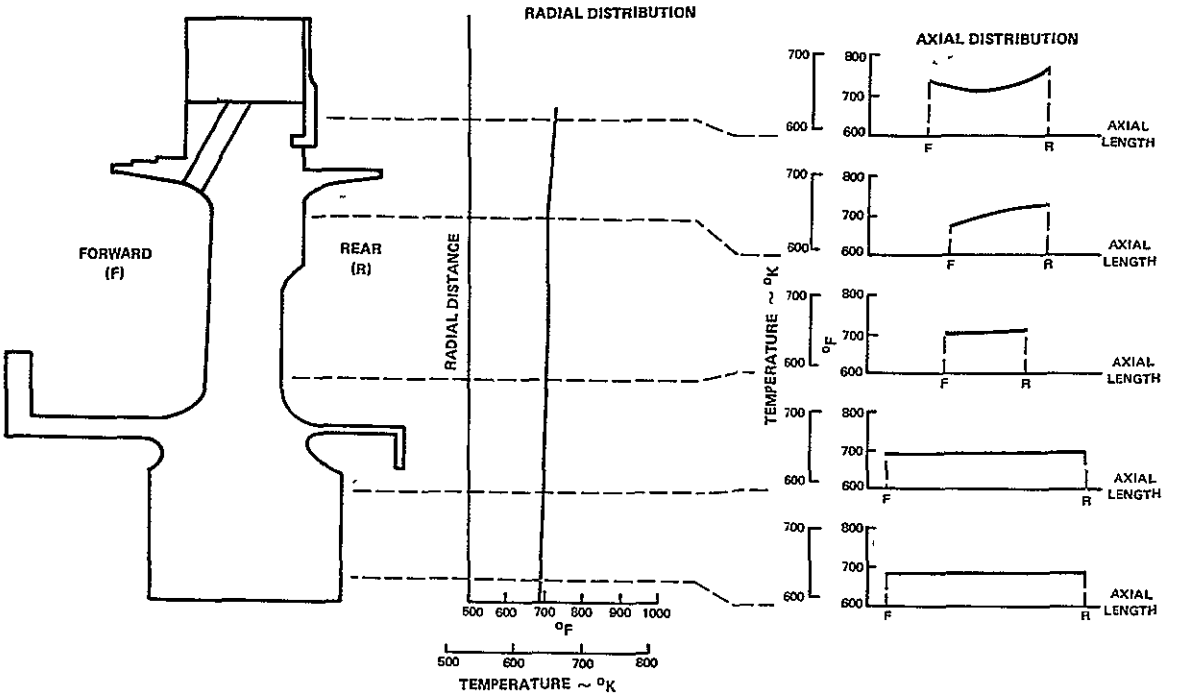

d. AT 1990 SECS
(LANDING)

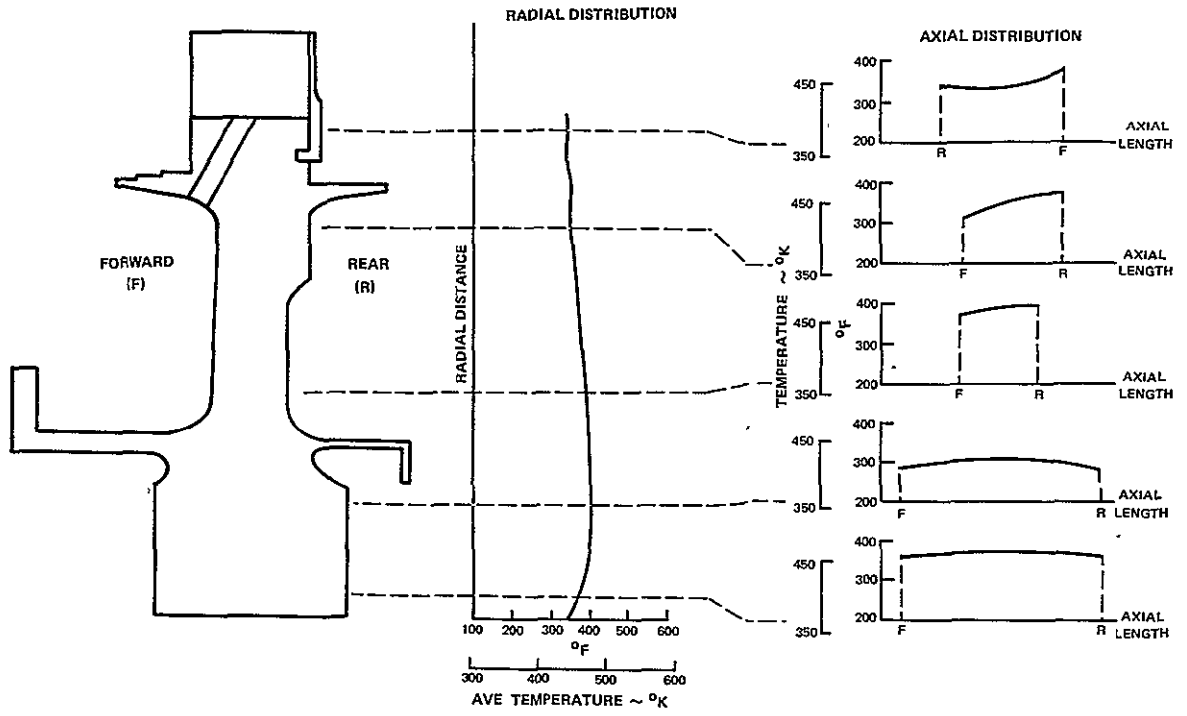

Figure 10 *Radial and Axial Temperature Distribution in Standard and Advanced Standard Disks at Pertinent Points in the Flight Cycle* (Cont)

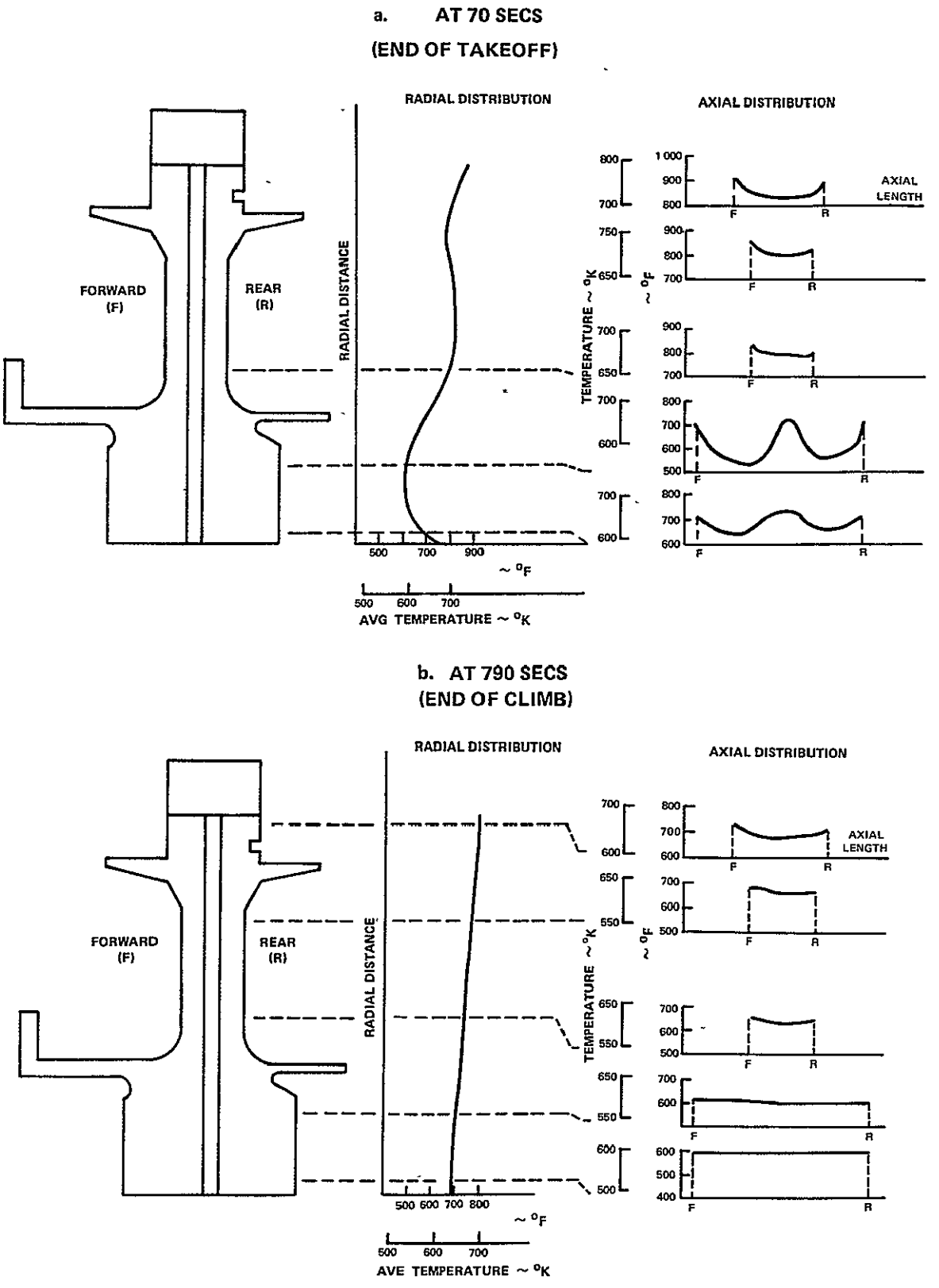

Figure 11 *Radial and Axial Temperature Distribution in the Design Disk at Pertinent Points in the Flight Cycle*

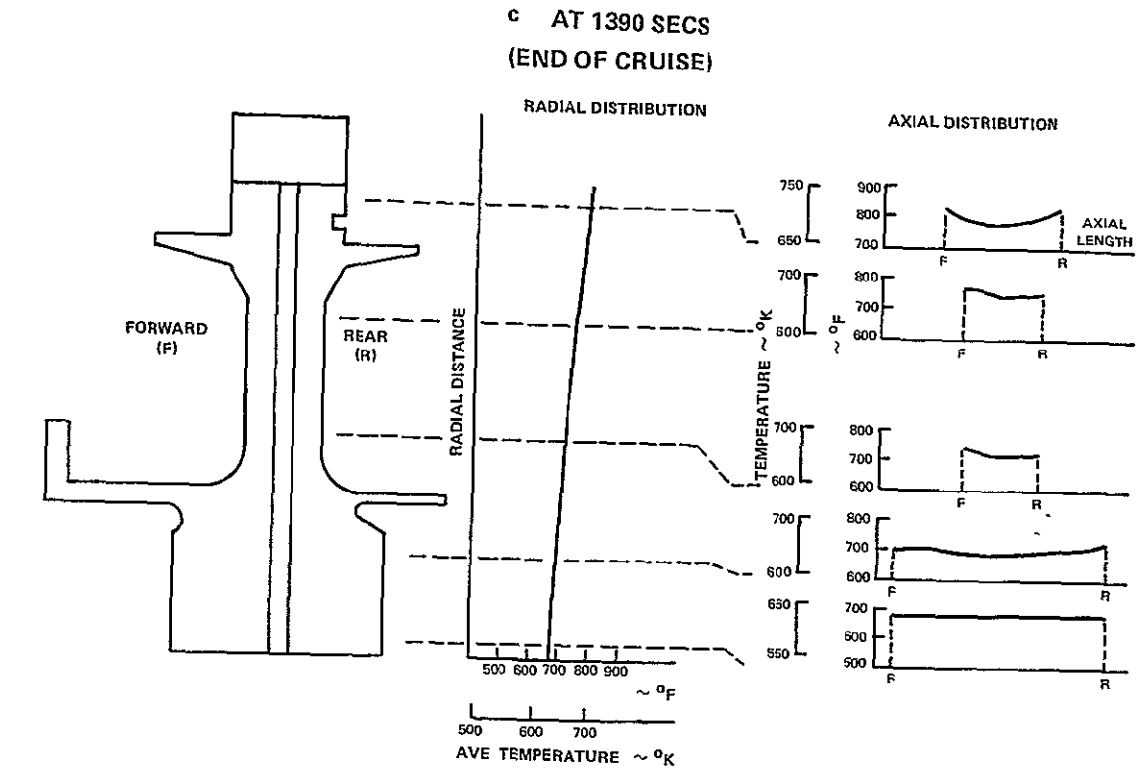

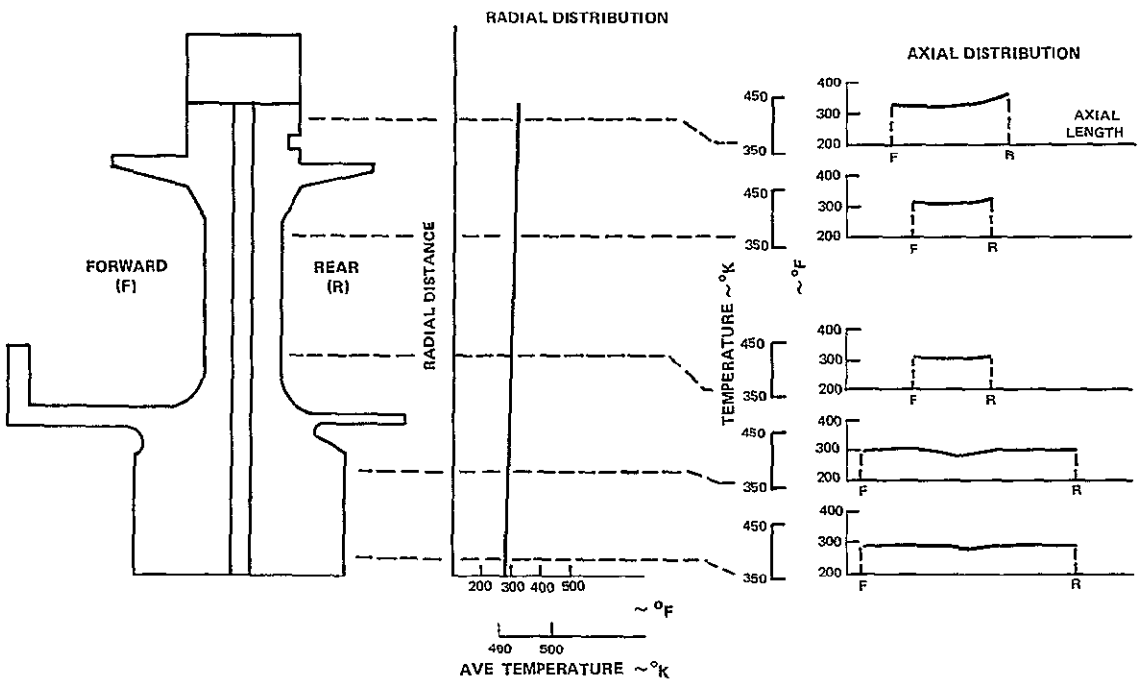

Figure 11 *Radial and Axial Temperature Distribution in the Design Disk at Pertinent Points in the Flight Cycle* (Cont)

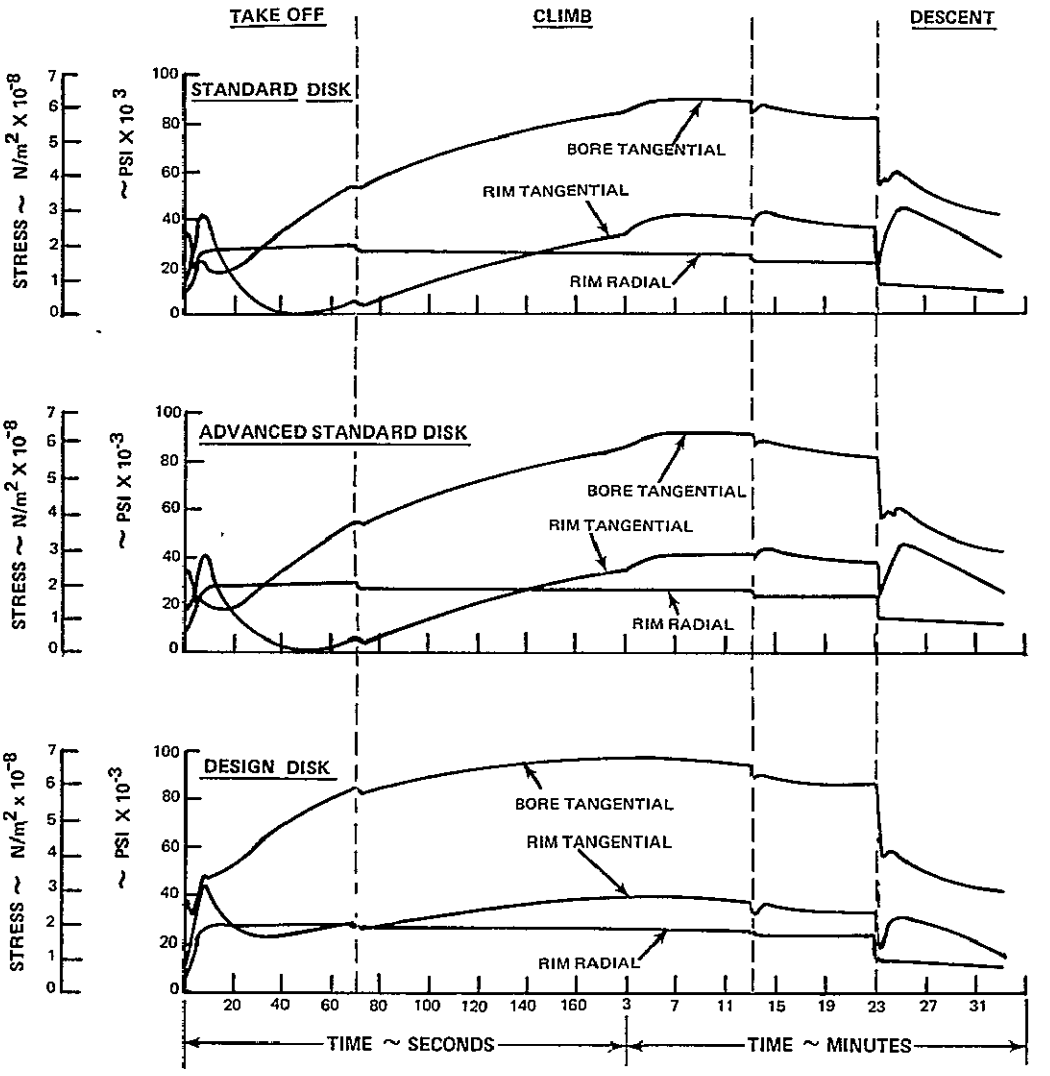

Figure 12 Nominal Disk Rim and Bore Stresses at Various Flight Conditions

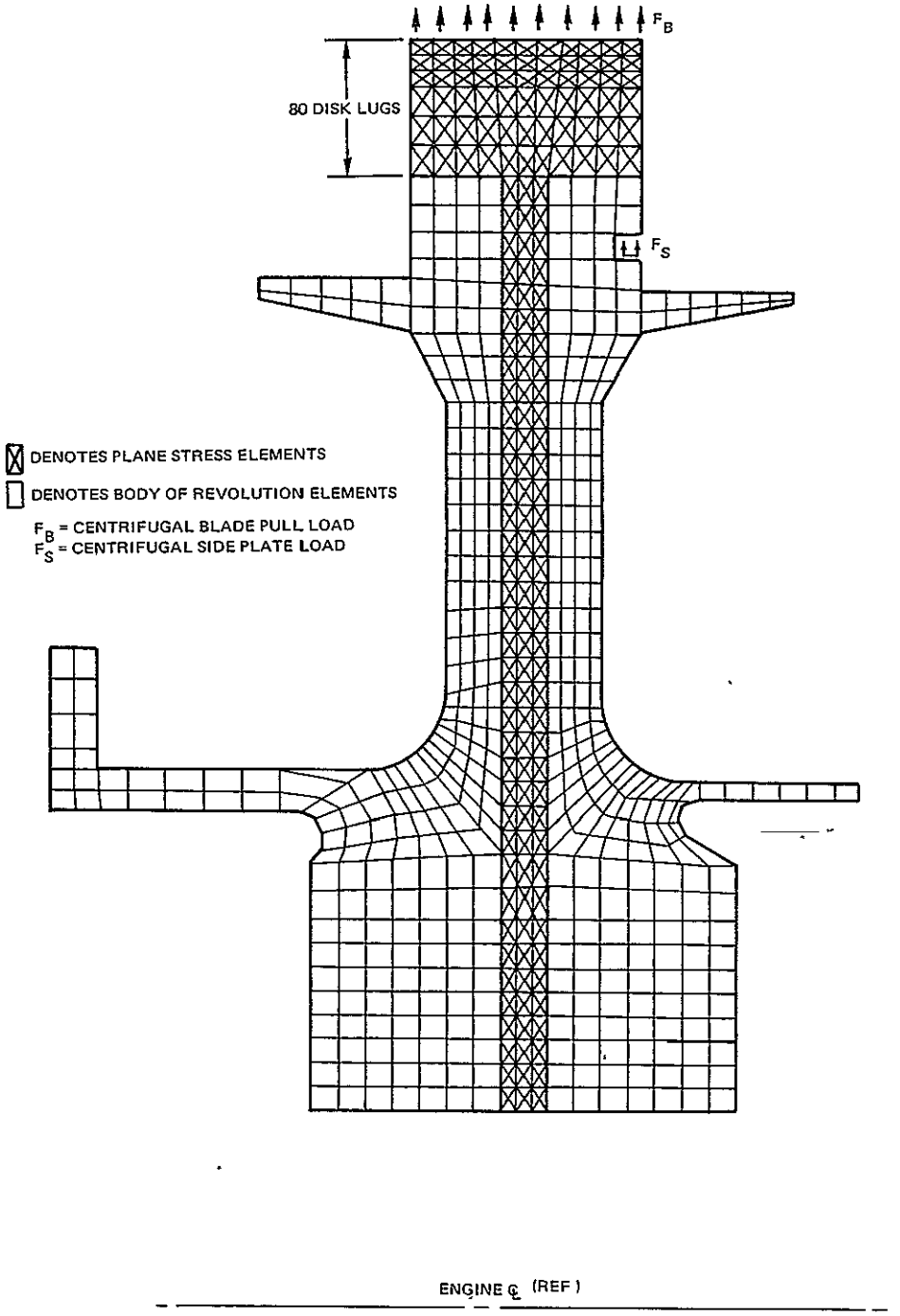

Figure 13 Finite Element Model of Design Disk

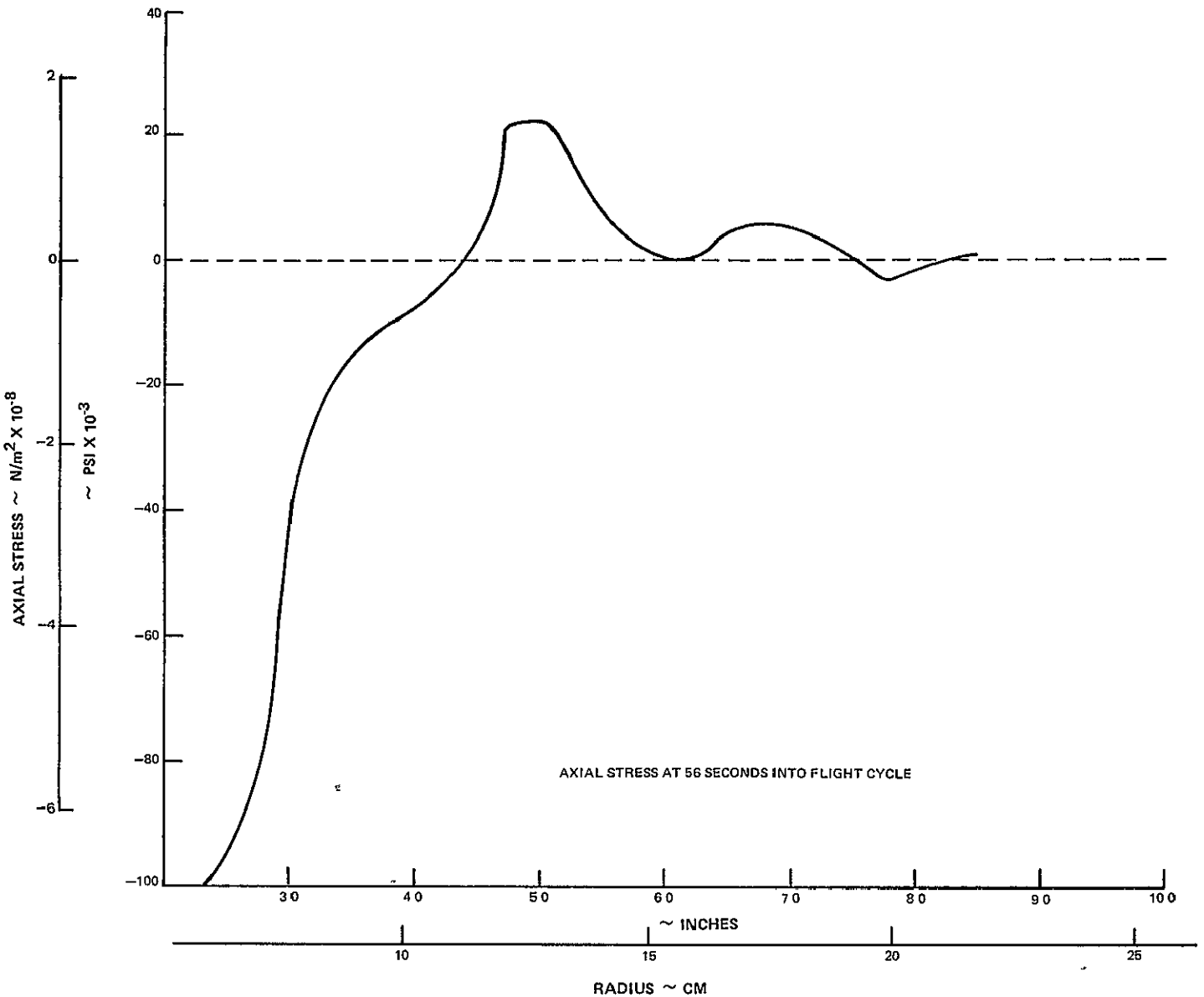

Figure 14 Design Disk Axial Stress vs Radius Along Bond Surface

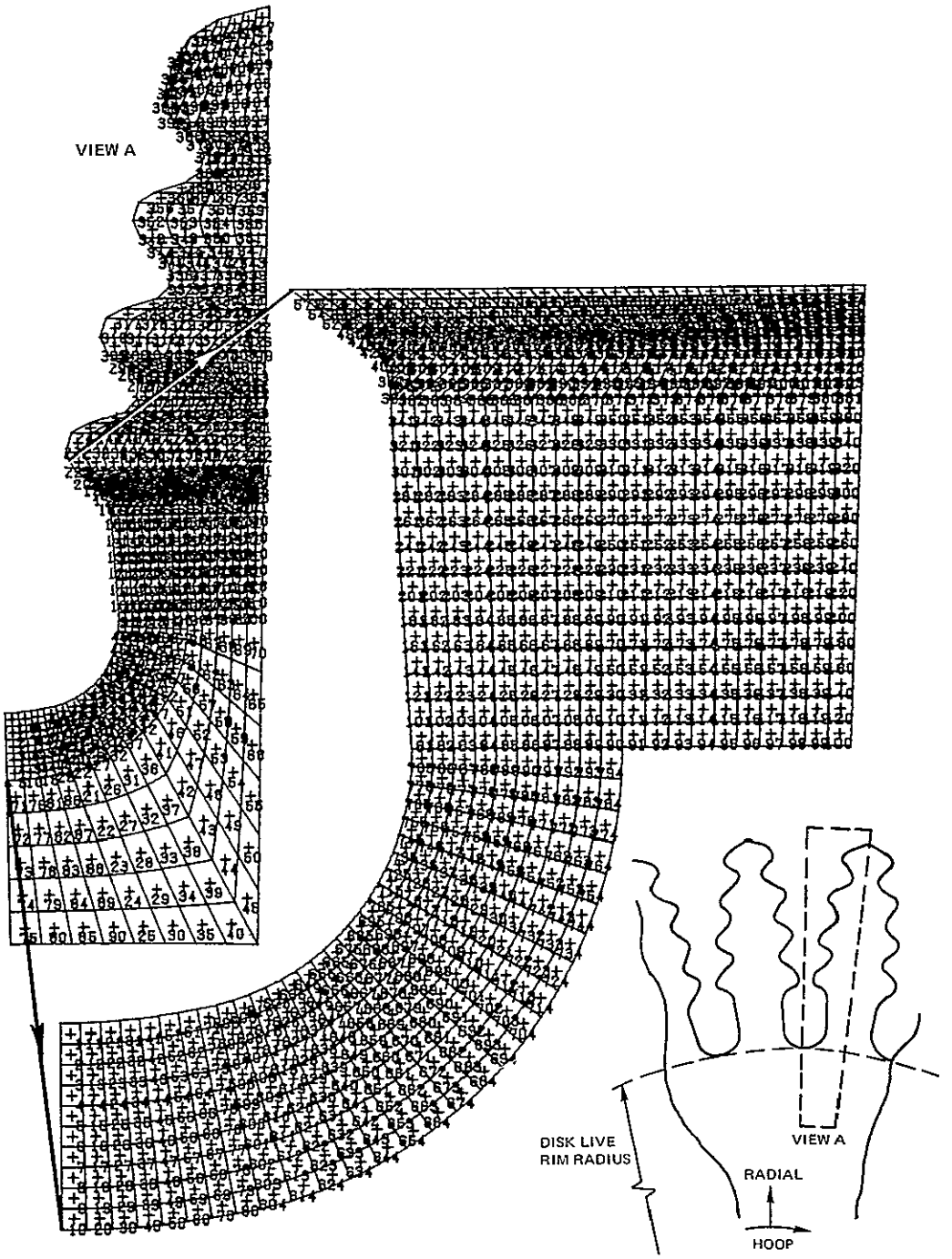

Figure 15 Finite Element Model of Design Disk Broach Slot

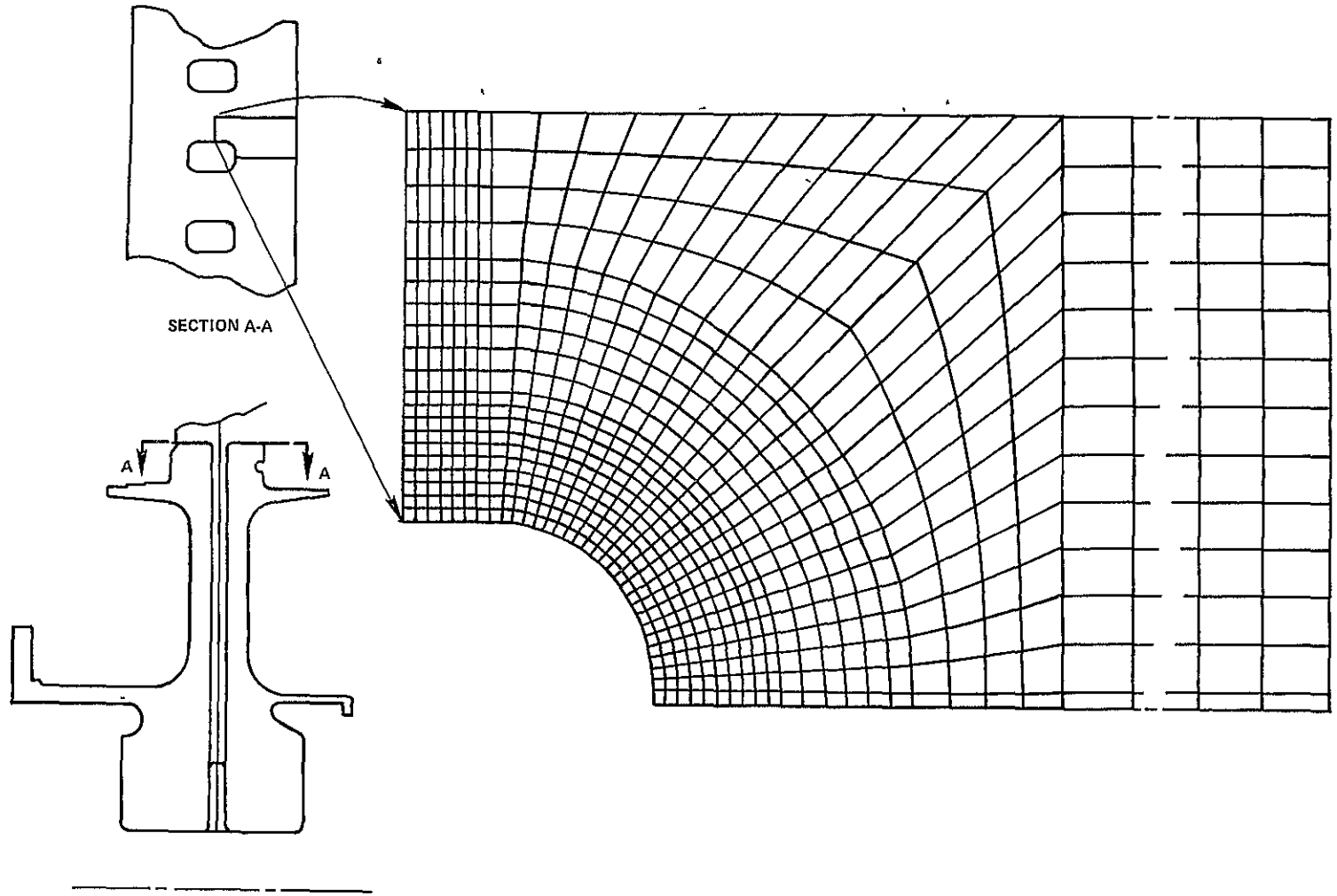

Figure 16 Finite Element Model of Design Disk Cooling Air Channel

BLADE ROOT CONNECTIONS

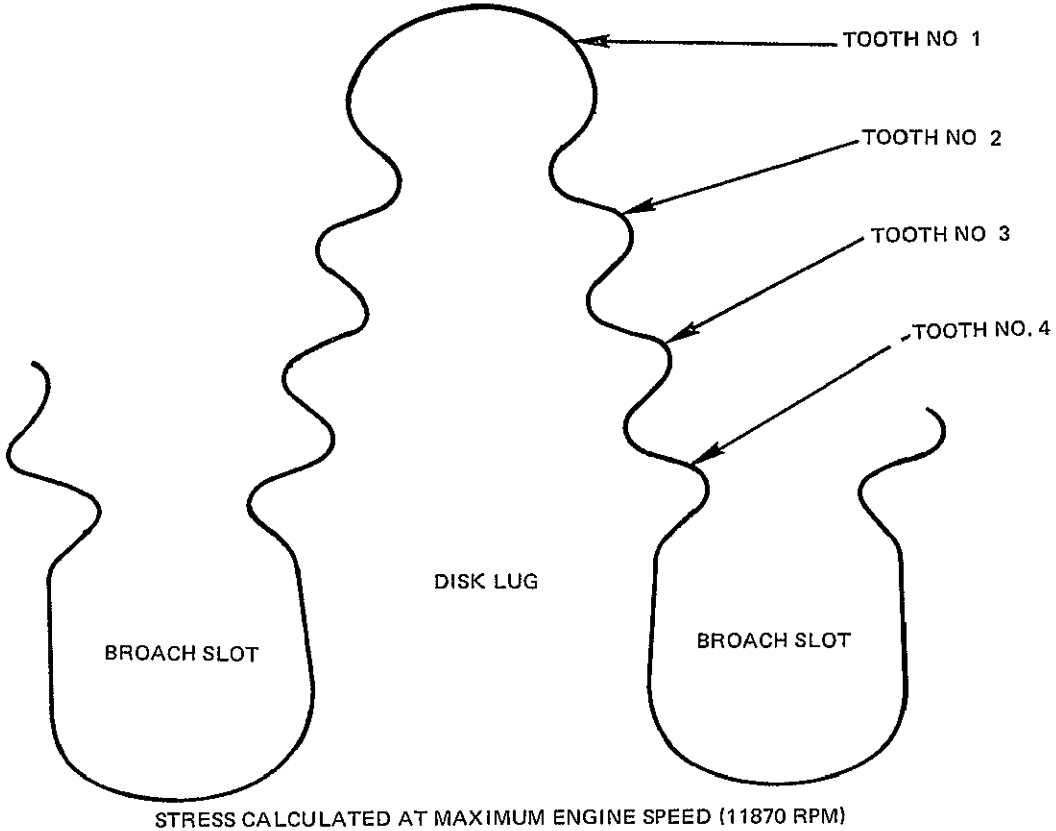

STRESS CALCULATED AT MAXIMUM ENGINE SPEED (11870 RPM)

TOOTH NO	TENSILE STRESS IN NECKS OF THE DISK LUG		TOOTH BEND STRESS		TOOTH SHEAR STRESS		TOOTH BEARING STRESS	
	10^8 N/m^2	KSI	10^8 N/m^2	KSI	10^8 N/m^2	KSI	10^8 N/m^2	KSI
1	2 01	29 1	1.84	26.7	1 52	22 0	4 33	62.8
2	2 55	37 0	1 57	22 7	1 50	21.7	4 15	60 2
3	2 79	40 4	1 56	22 6	1 50	21 7	4 15	60 2
4	2 94	42.6	2 68	38 9	1 34	19 4	4 47	64.8

Figure 17 Centrifugal Stresses at the Disk/Blade-Root Connection

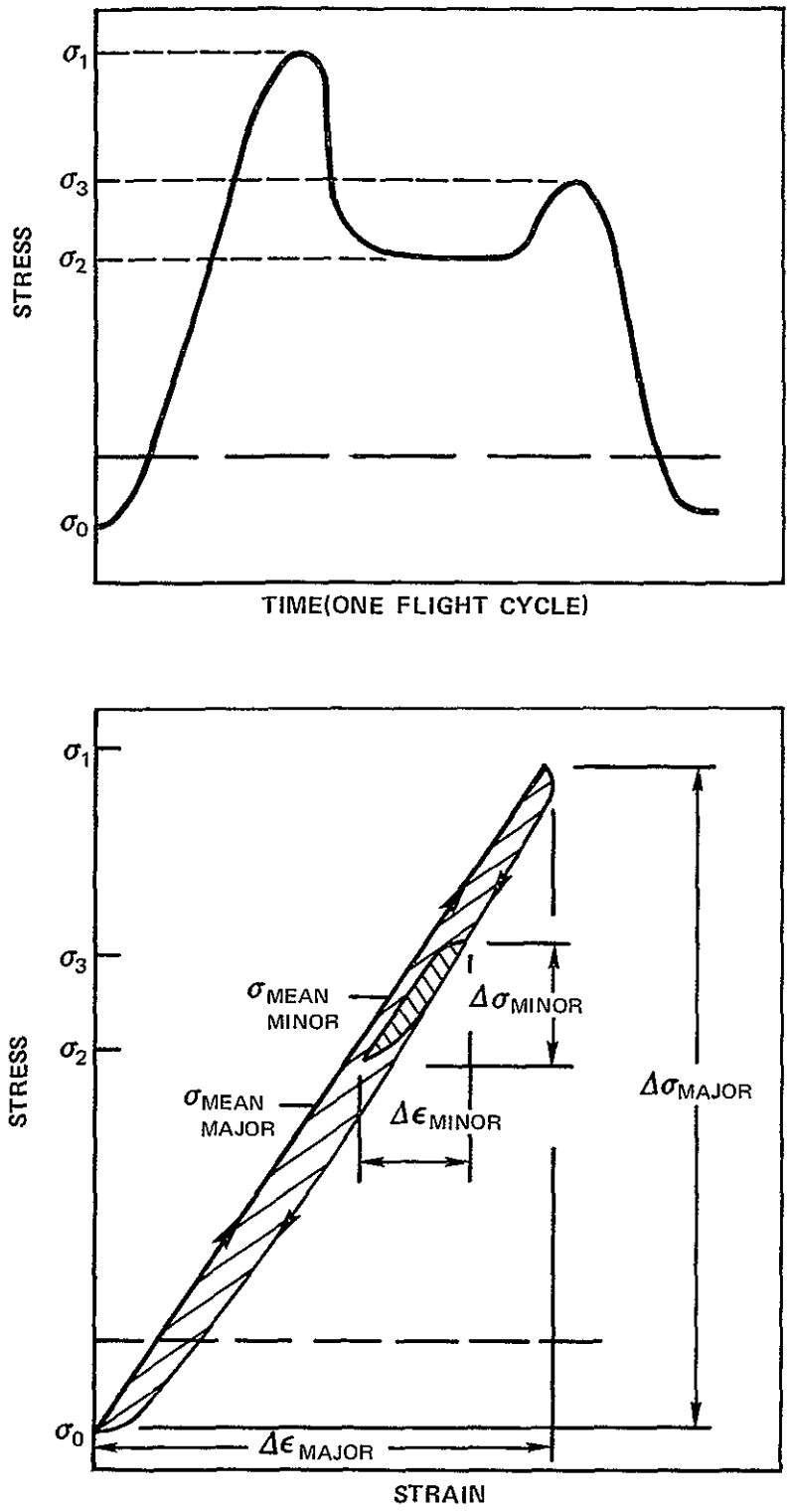

Figure 18 Stress History at Each Stress Concentration Location

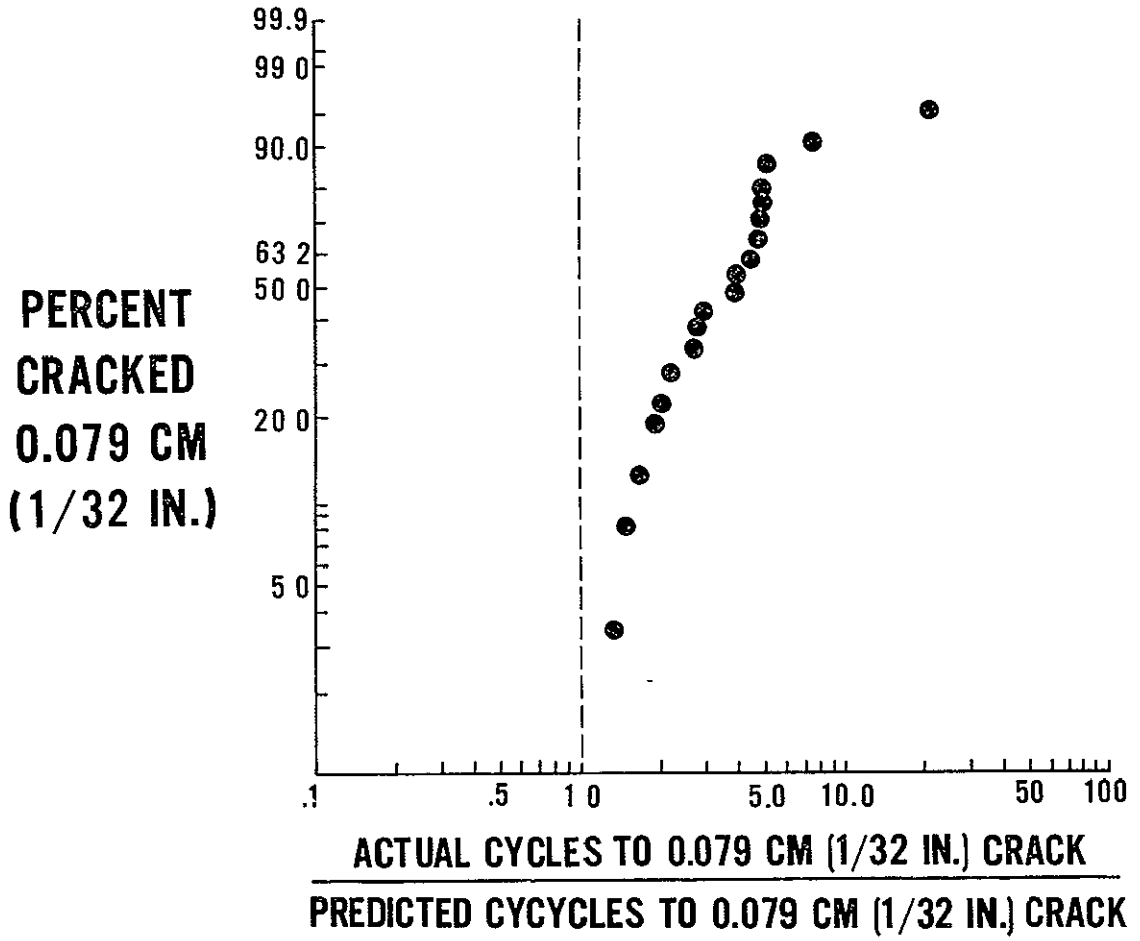

Figure 19 P&WA Engine Low Cycle Fatigue – Experience Vs. Prediction

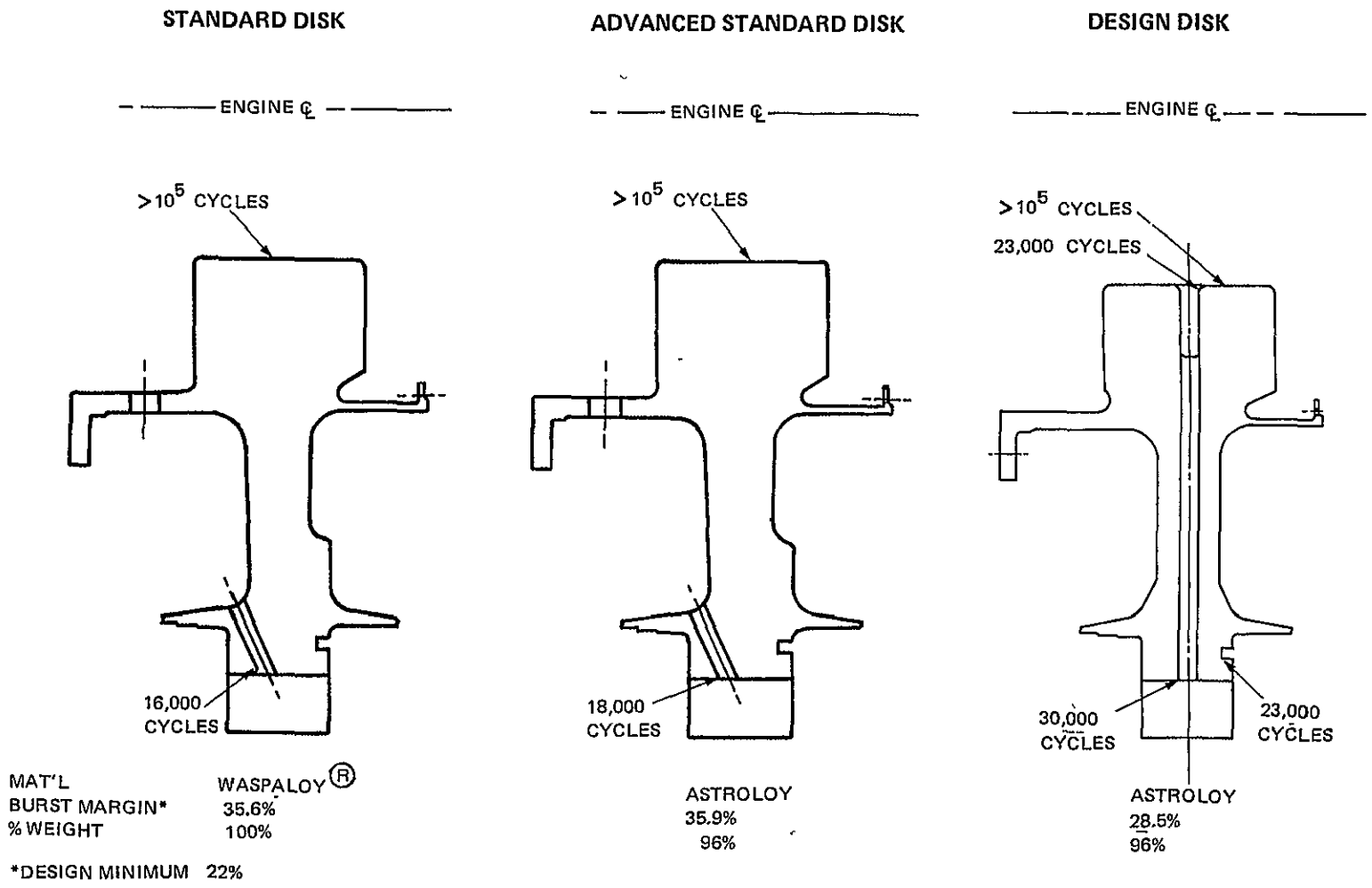

Figure 20 LCF Crack Initiation Life Summary of the Standard, Advanced Standard and Design Disks

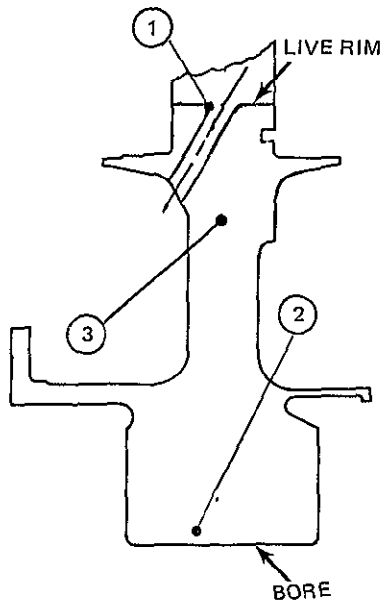

STANDARD DISK (WASPALOY)®

FLAW LOCATION

1. CRITICAL LOW CYCLE FATIGUE INITIATED FLAW SITE AT COOLING AIR HOLE EXIT
2. CRITICAL MANUFACTURING FLAW AT DISK BORE
3. CRITICAL MANUFACTURING FLAW AT DISK WEB MAXIMUM RADIAL STRESS LOCATION

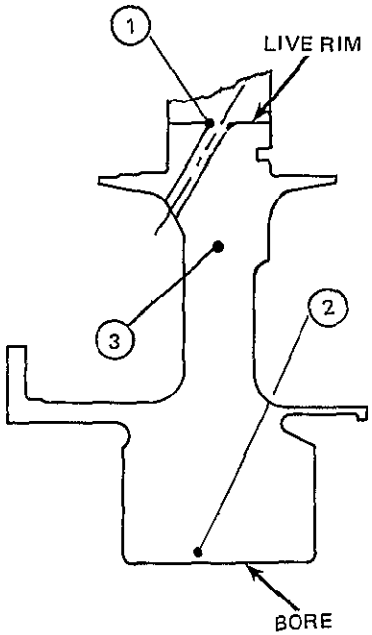

ADVANCED STANDARD DISK (ASTROLOY)

FLAW LOCATION

1. CRITICAL LOW CYCLE FATIGUE INITIATED FLAW SITE AT COOLING AIR HOLE EXIT
2. CRITICAL MANUFACTURING FLAW AT DISK BORE
3. CRITICAL MANUFACTURING FLAW AT DISK WEB MAXIMUM RADIAL STRESS LOCATION

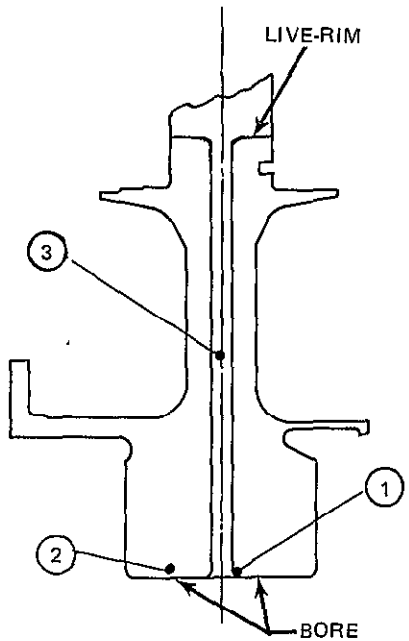

DESIGN DISK (ASTROLOY)

FLAW LOCATION

1. CRITICAL LOW CYCLE FATIGUE INITIATED FLAW SITE AT COOLING AIR CHANNEL ENTRANCE
2. CRITICAL MANUFACTURING FLAW AT DISK BORE
3. CRITICAL MANUFACTURING FLAW AT TLP® BOND LINE IN RADIAL VANE

Figure 21 Critical Flaw-Sites for the Standard, Advanced Standard and Improve Design Disks

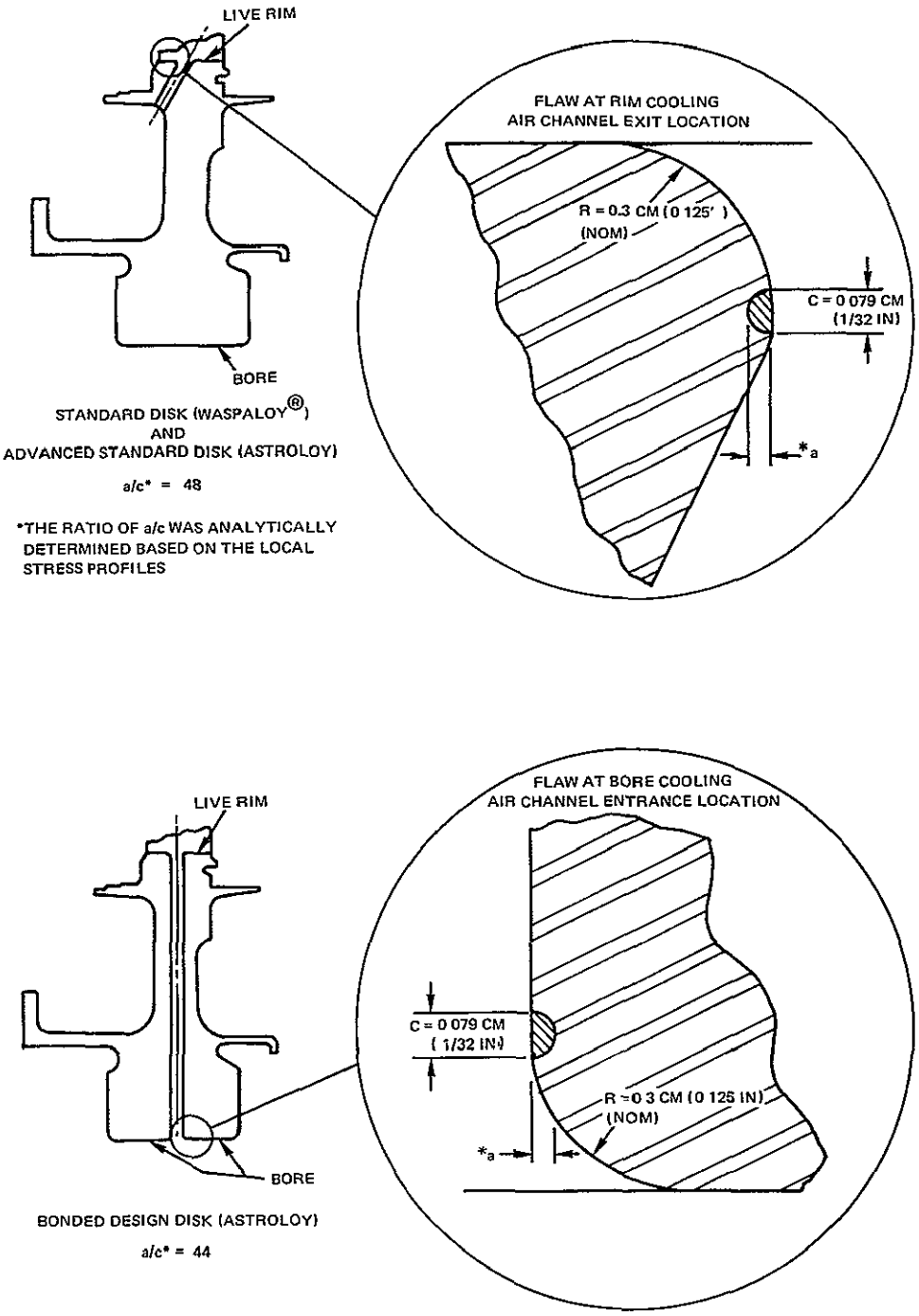

Figure 22 LCF Initiated Flaws for the Standard, Advanced Standard and Design Disks

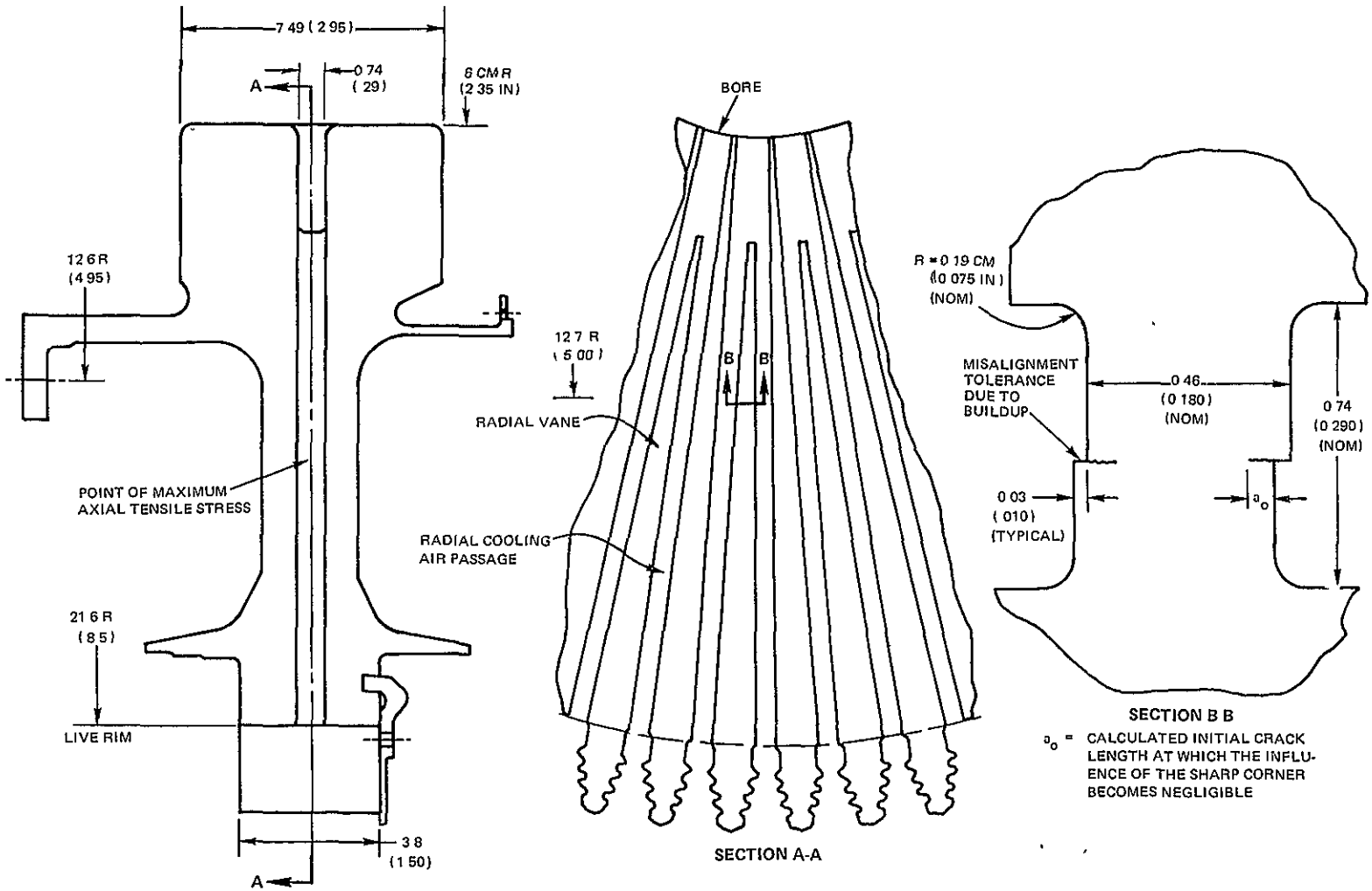

Figure 23 Schematic of Design Disk Showing TLP® Bond Misalignment

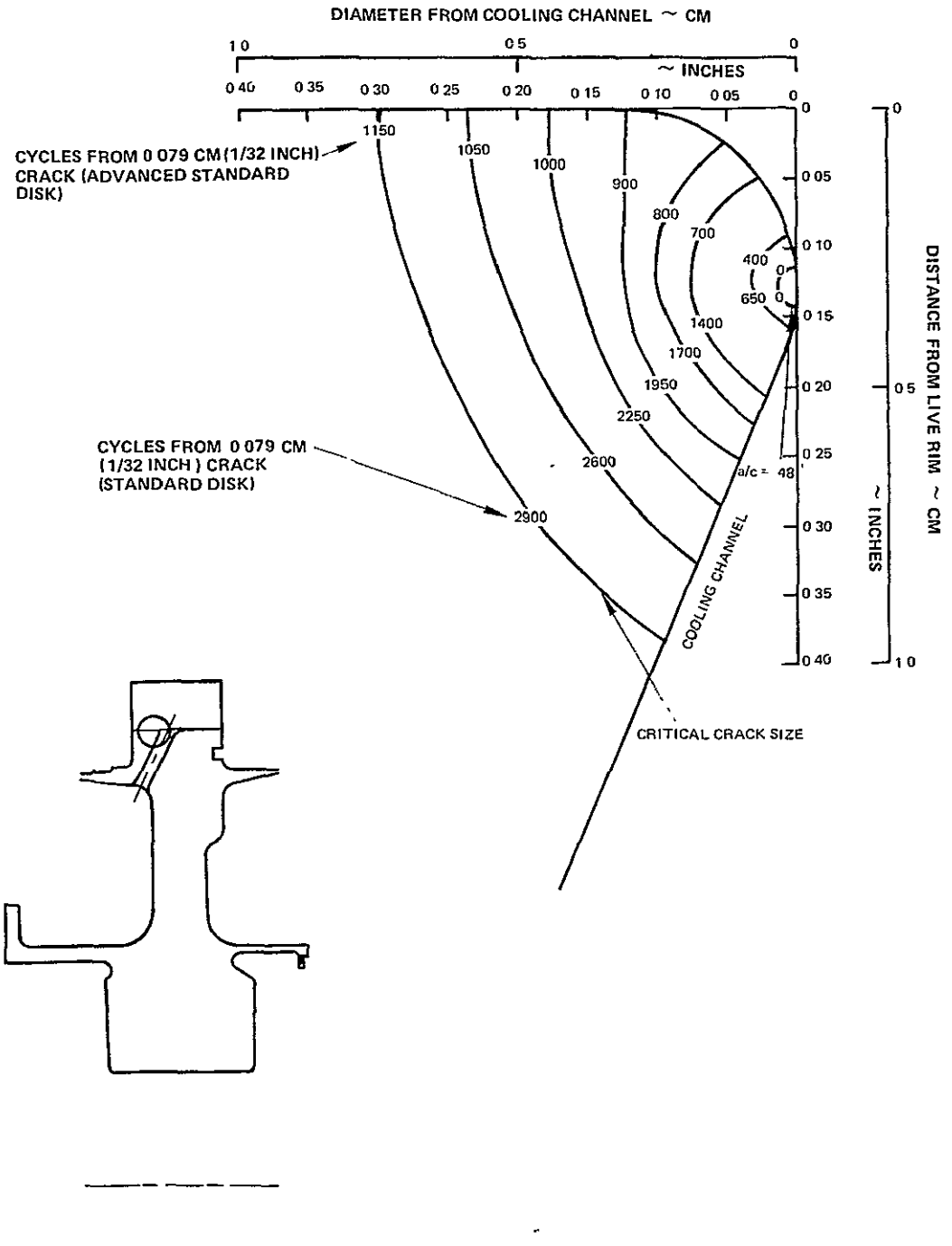

Figure 24 *Crack Profiles for Standard and Advanced Standard Disk Cooling-Air Channel Exit Cracks*

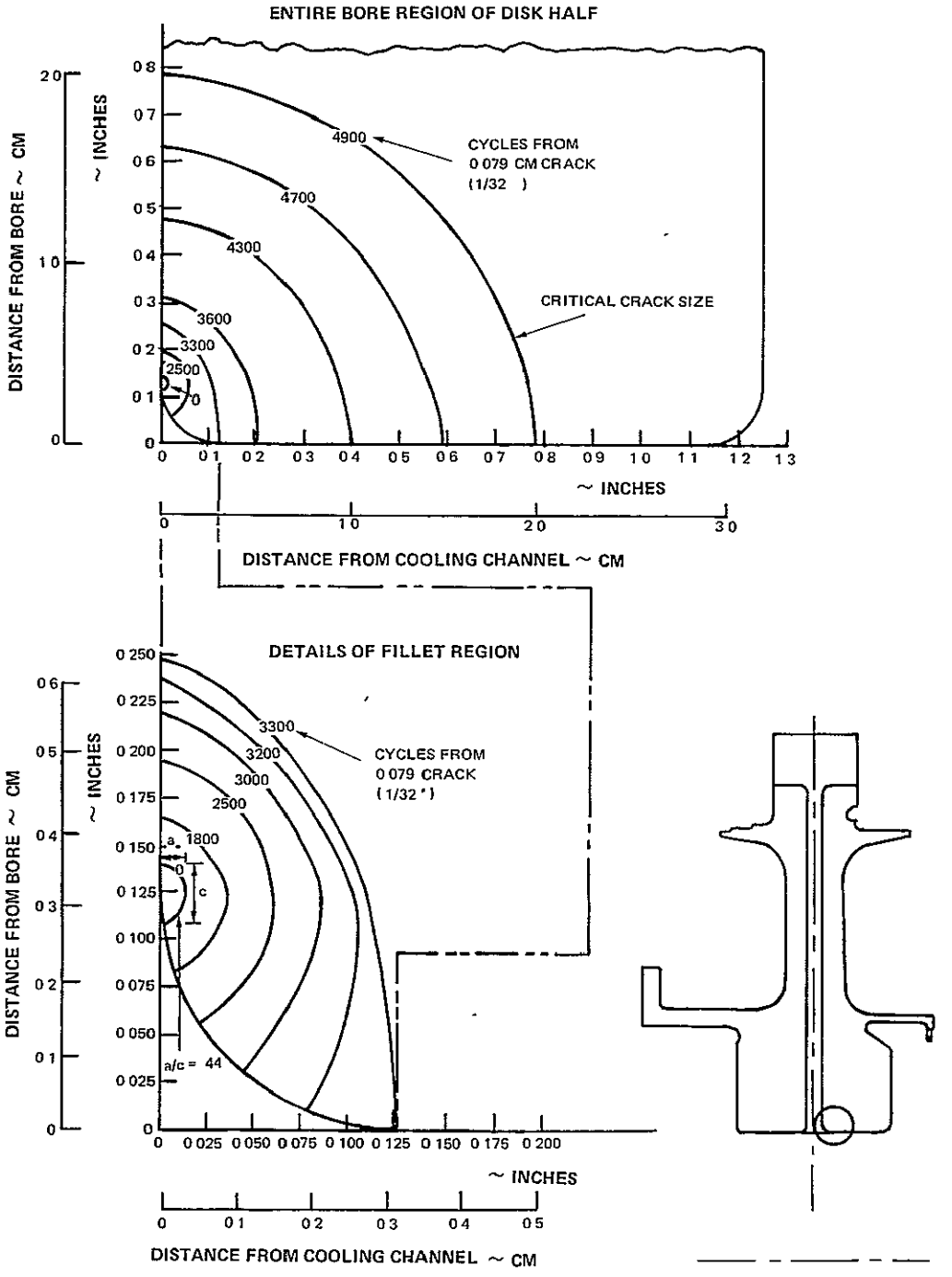

Figure 25 Crack Profiles for Design Disk Cooling-Air Channel Entrance Crack

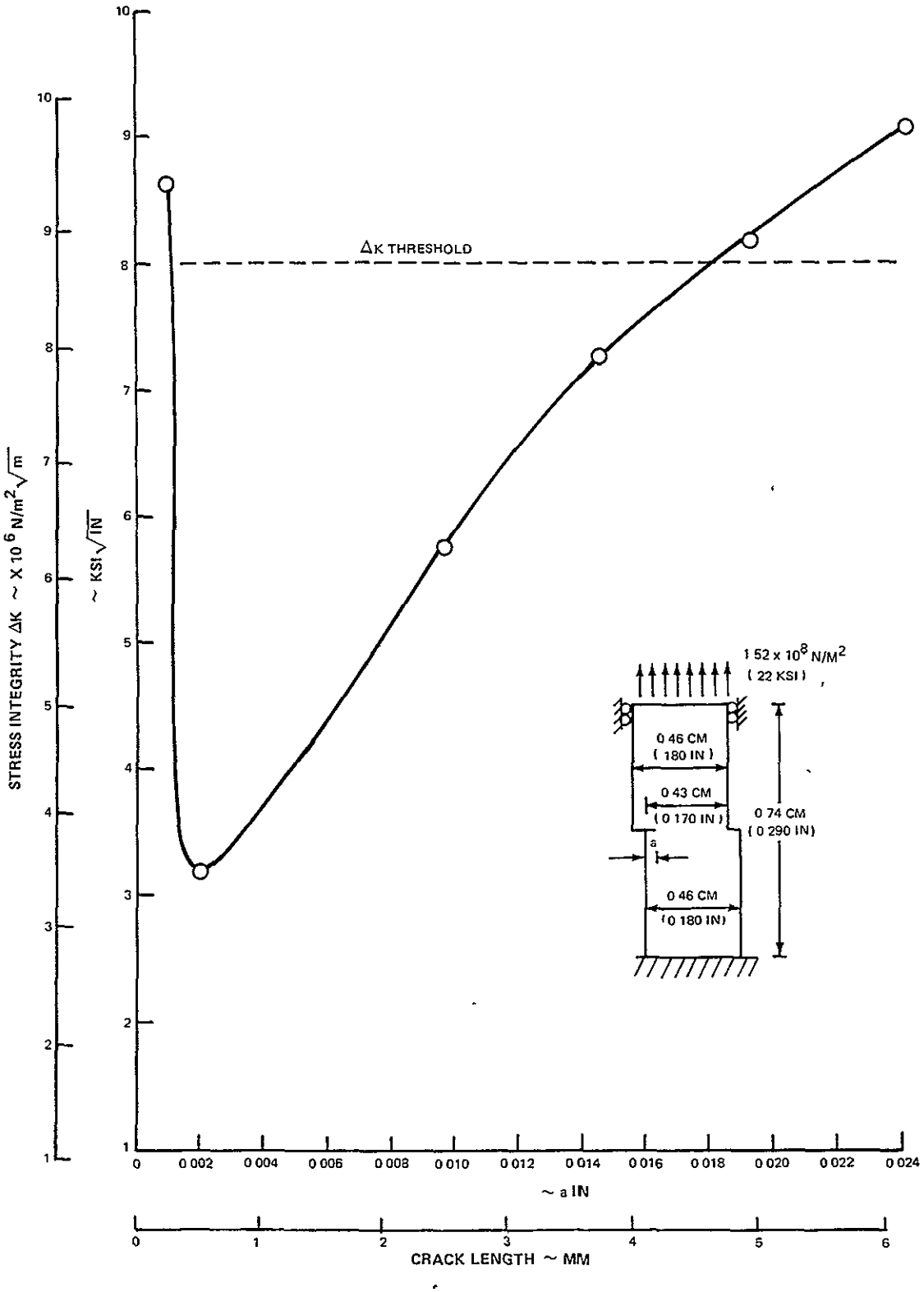

Figure 26 Stress Intensity (ΔK) Values for Bond Misalignment in Web of Design Disk

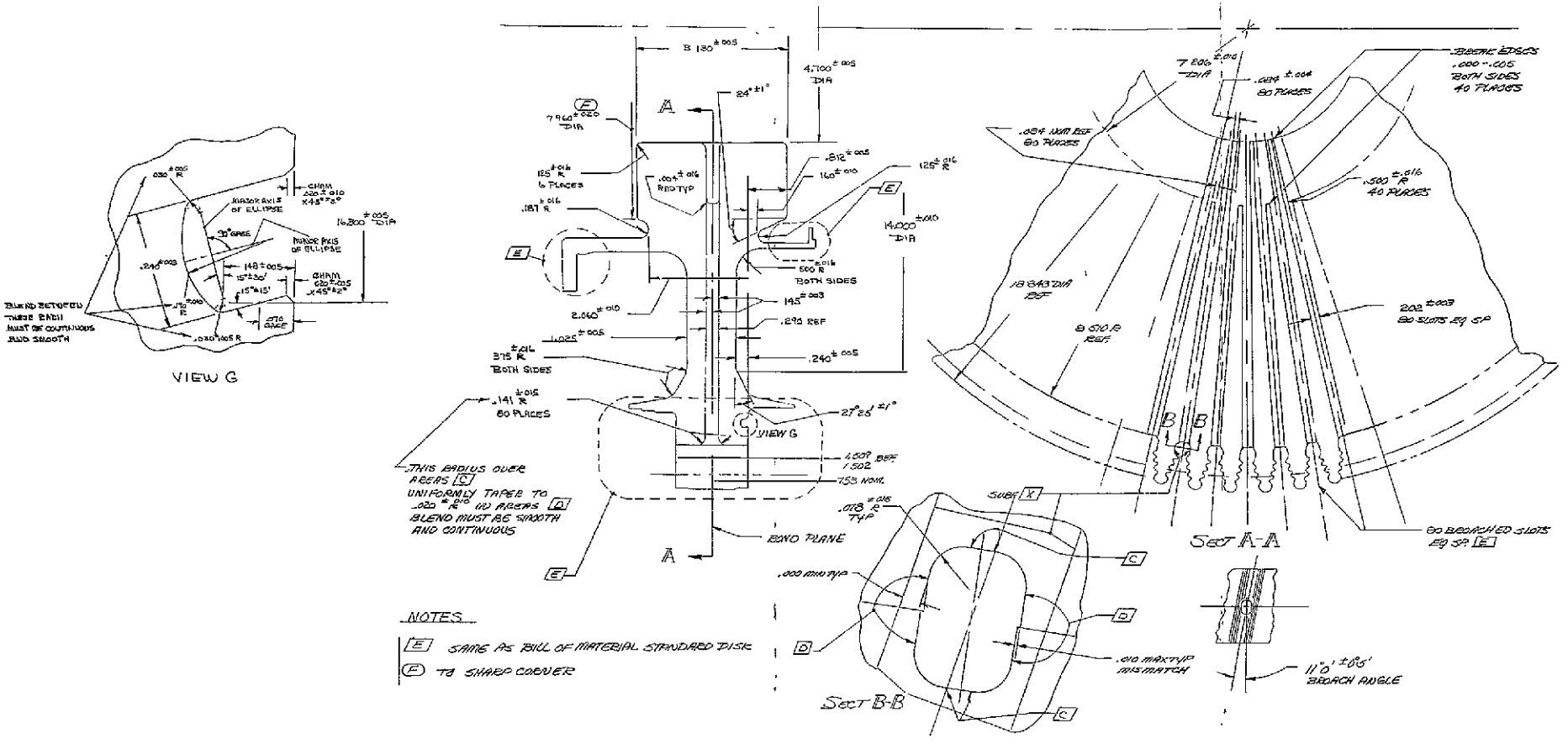

Figure 27 JT8D-17 First-Stage High Pressure Turbine Bore-Entry-Cooled Improved Design Disk

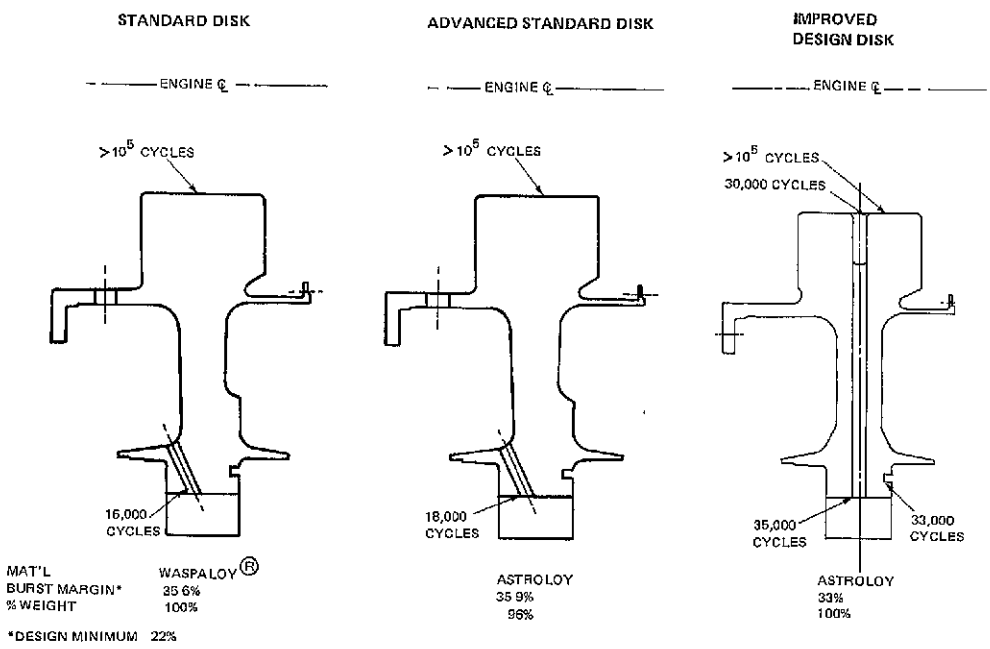

Figure 28 LCF Crack Initiation Life Summary of the Standard, Advanced Standard and Improved Design Disks

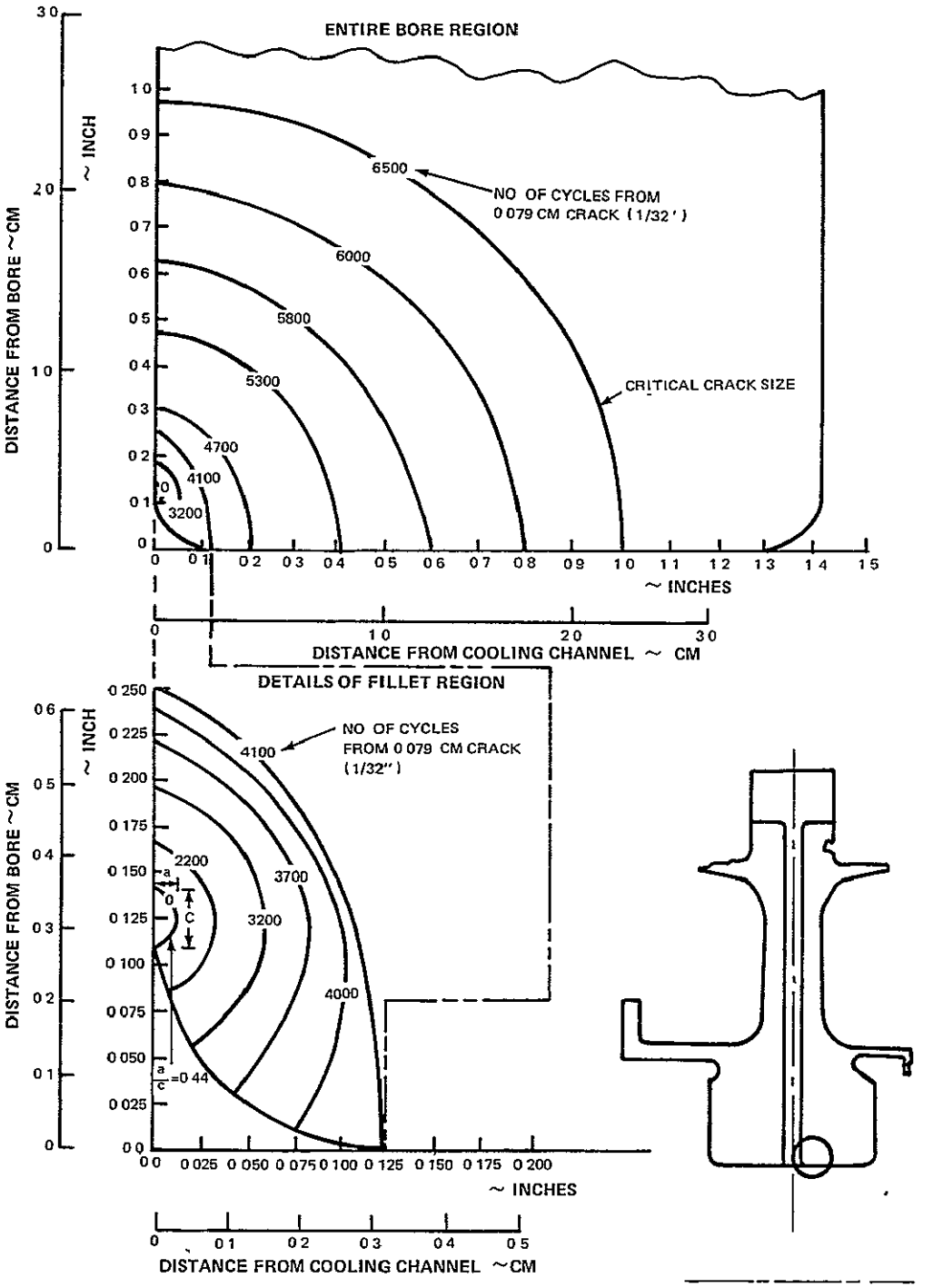

Figure 29 *Crack Profiles for the Improved Design Disk Cooling-Air Channel Entrance Crack*

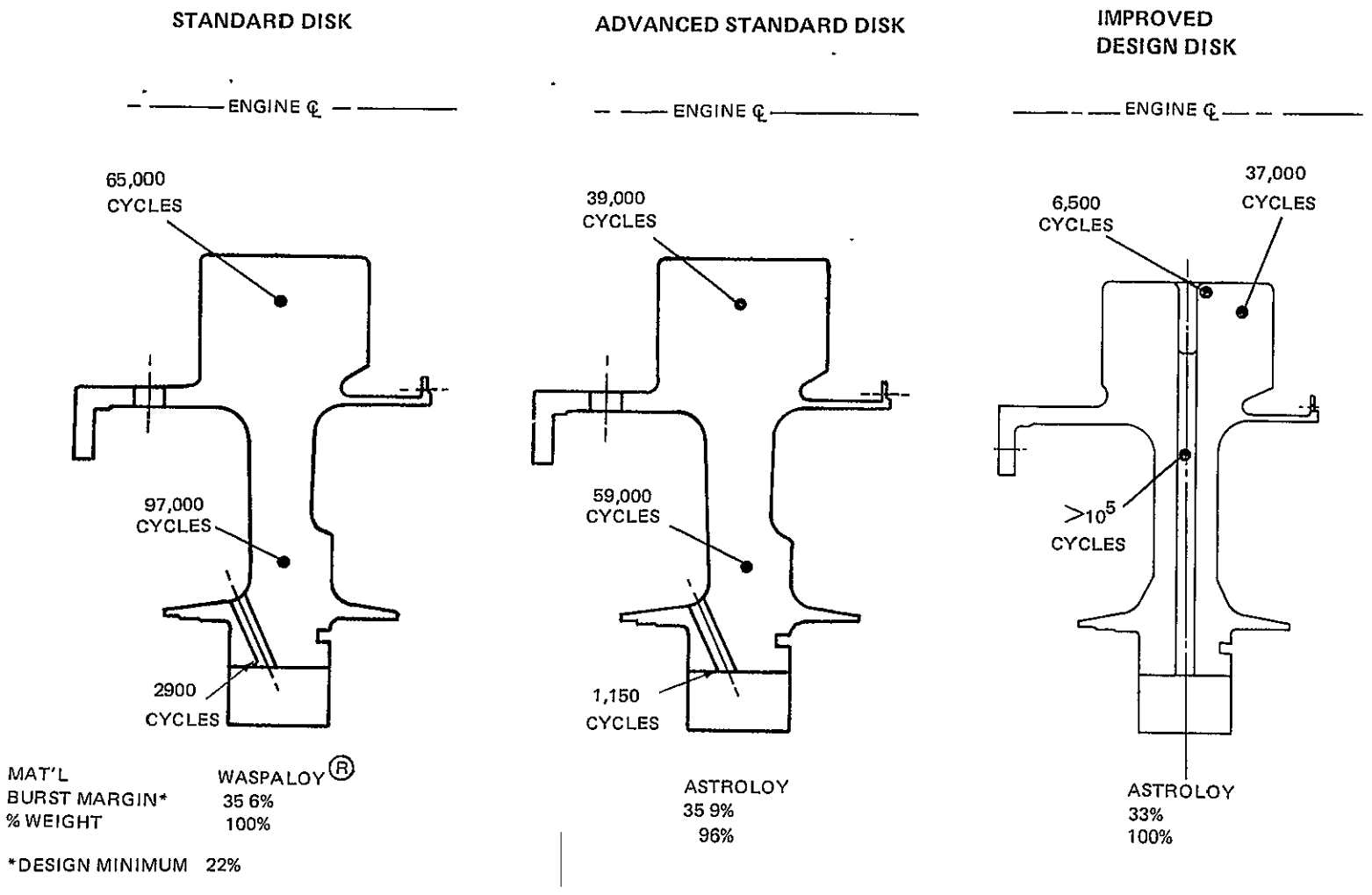

Figure 30 *Crack Propagation Life Summary of the Standard, Advanced Standard and Improved Design*

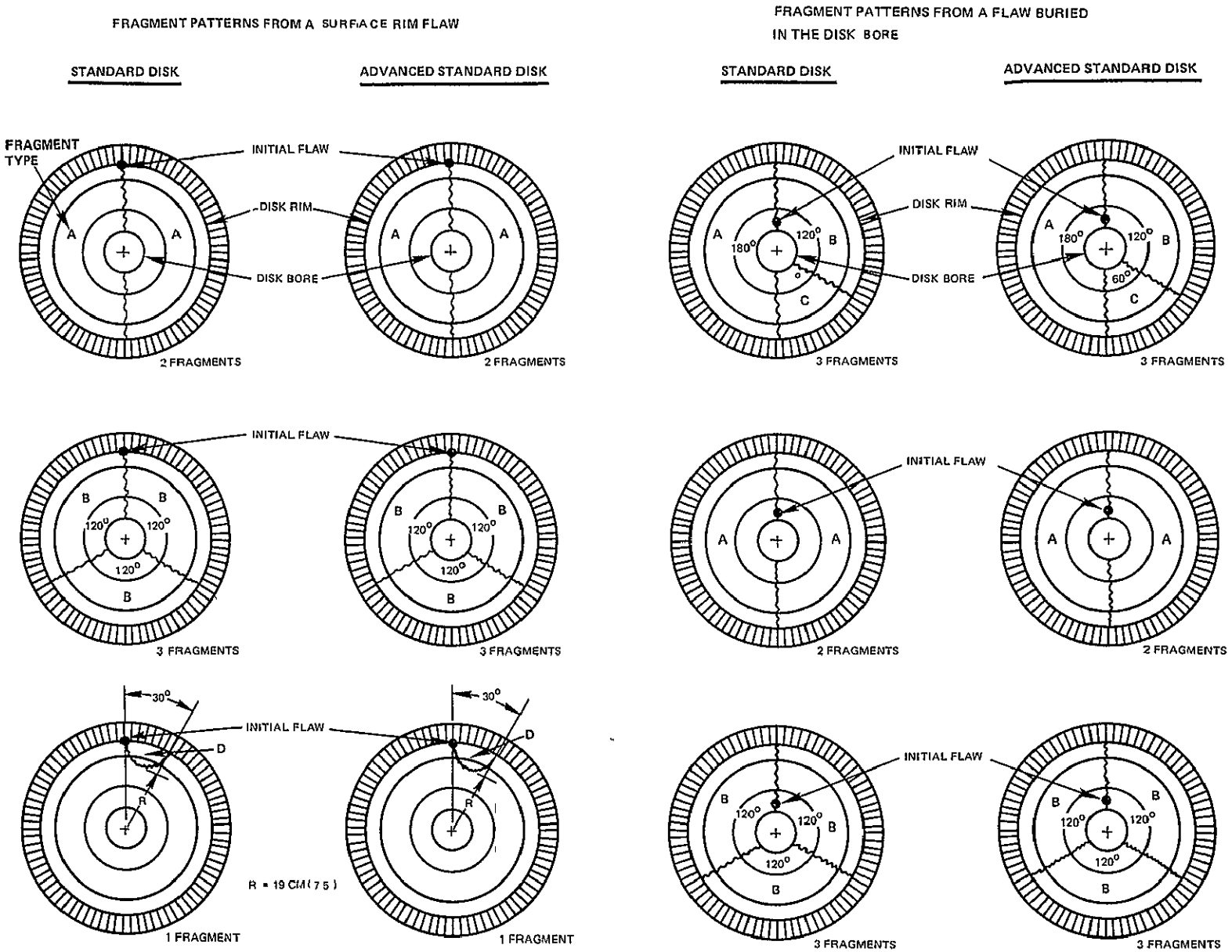

Figure 31 *Assumed Fragment Patterns for the Standard and Advanced Standard Disks*

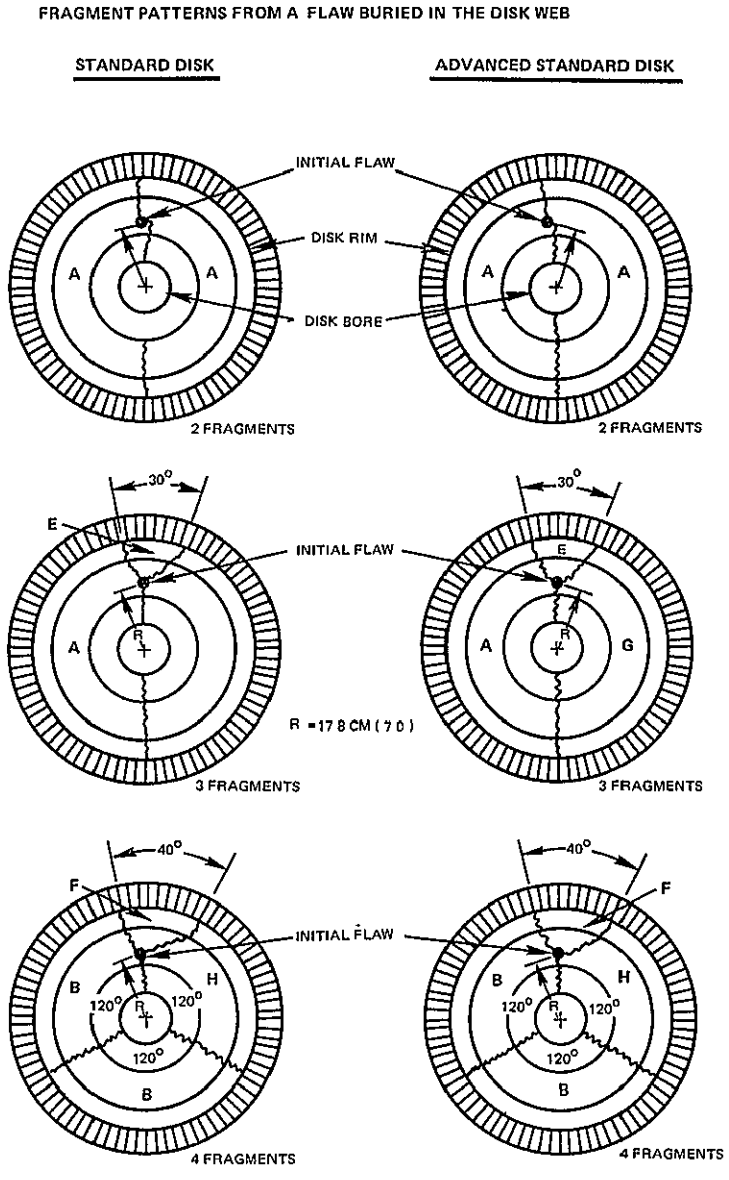

FRAGMENT TYPE	TOTAL FRAGMENT ENERGY @ 11870 RPM			
	STANDARD DISK		ADVANCED STANDARD DISK	
	JOULES 10^6	IN–LB 10^6	JOULES 10^6	IN–LB 10^6
A	1 02	9 01	980	8 68
B	.679	6.01	654	5 78
C	339	3.0	327	2 89
D	133	1 17	.128	1 13
E	.078	690	075	665
F	105	934	.102	900
G	940	8 32	.905	8 01
H	573	5 07	552	4 88

Figure 31 Assumed Fragment Patterns for the Standard and Advanced Standard Disks (Cont'd)

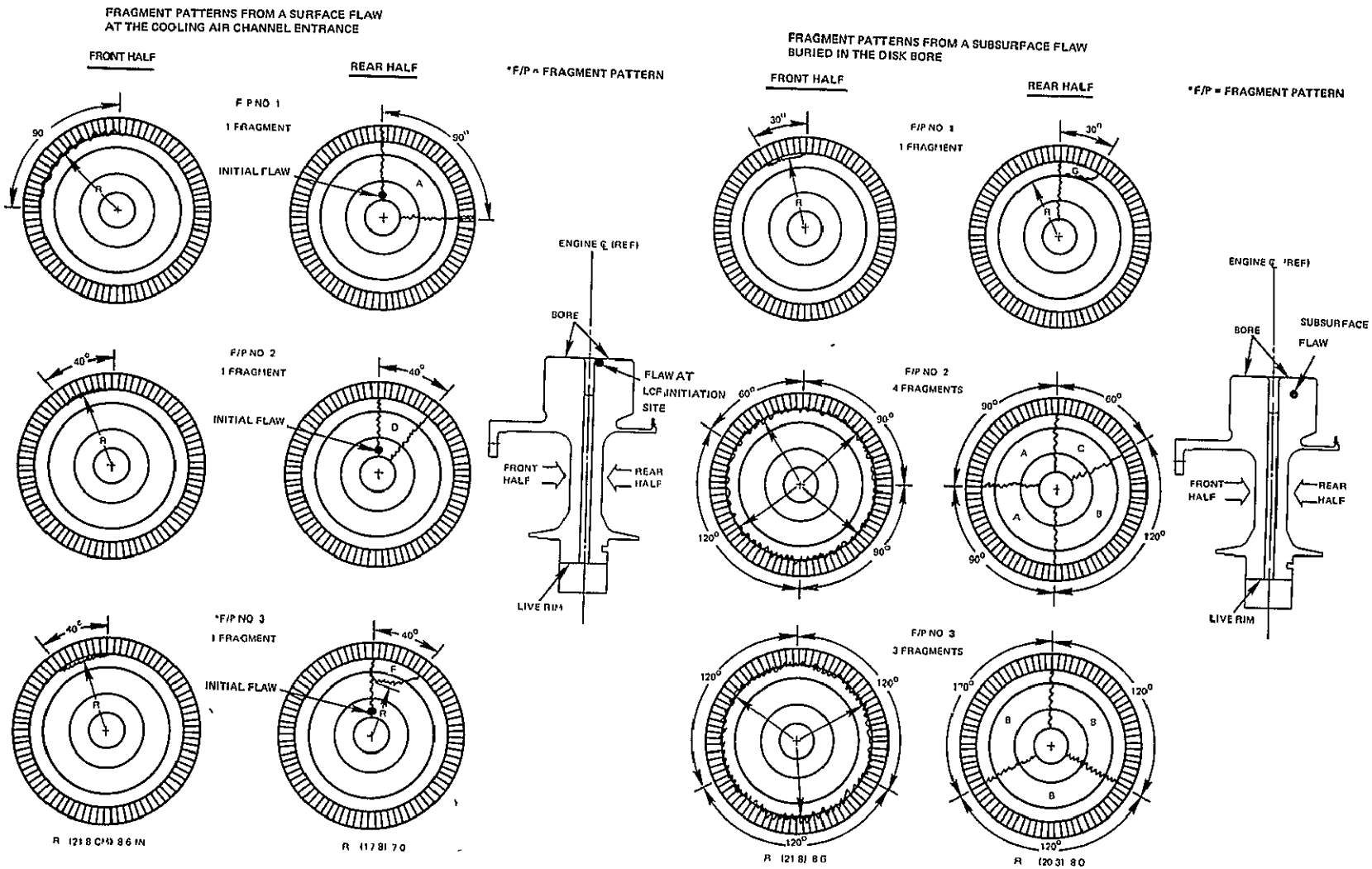

Figure 32 *Assumed Fragment Patterns for the Improved Design Disk*

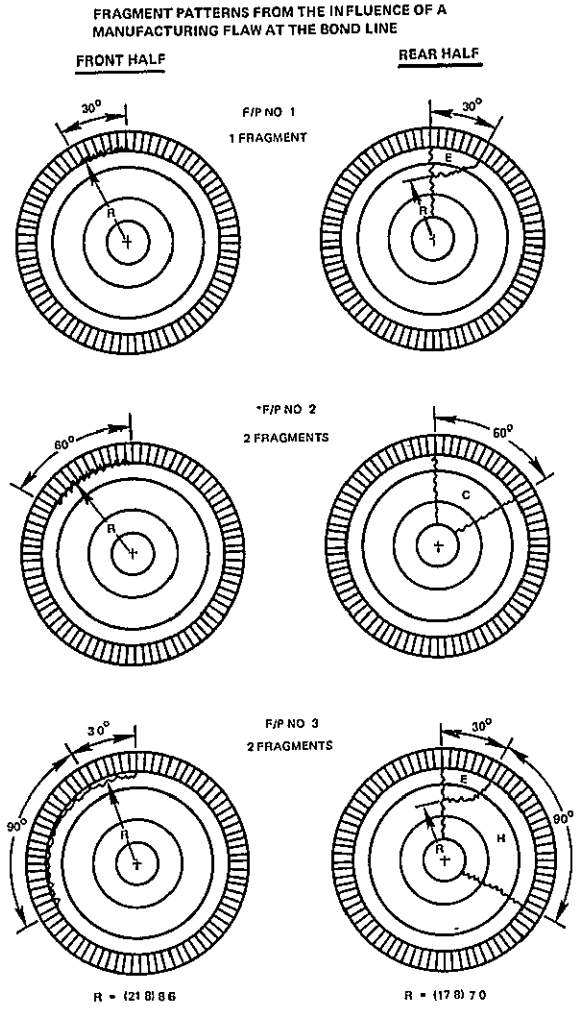

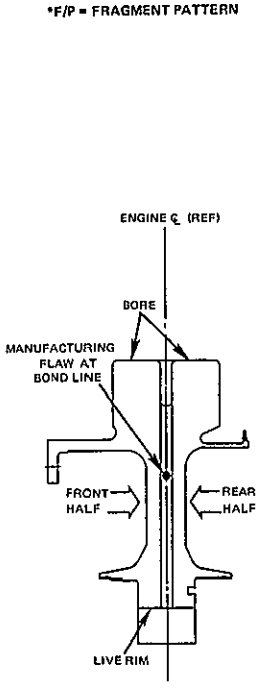

TOTAL FRAGMENT ENERGY @ 11870 RPM

FRAGMENT TYPE	DESIGN DISK	
	JOULES 10^6	IN-LB 10^6
A	385	3.40
B	.513	4 54
C	256	2 27
D	171	1 51
E	.072	633
F	097	855
G	064	.570
H	441	3.91

Figure 32 Assumed Fragment Patterns for the Improved Design Disk (Cont'd)

LIST OF SYMBOLS

a/c	crack depth to crack length (surface crack)
B/M	Bill-of-Material
BTU	British Thermal Units
cm	centimeters
°F	degrees Fahrenheit
ID	inner diameter
in	inches
J	Joules
°K	degrees Kelvin
Kg	kilograms
ksi	1000 pounds per square inch
LCF	low cycle fatigue
m	meters
mm	millimeters
N	Newtons
psi	pounds per square inch
RPM	revolutions per minute
SCF	stress concentration factor
TLP®	Transient Liquid Phase bonding process
ΔK	stress intensity factor
ϵ	strain

DISTRIBUTION LIST

Commanding Officer
U. S. Army Air Mobility and Dev. Lab.
Fort Eustis, VA 23604
Attn Leroy Burrows 1

Commanding Officer
Ballistic Research Laboratories (USA-ARDC)
Aberdeen Proving Ground, MD 21005
Attn AMXRD-BAM
N. J. Huffington, Jr 1
J Santiago 1

Commanding Officer
U S. Army Materials and Mechanics Research Center
Watertown, MA 02172
Attn AMXMR-ED
J Adachi 1
J. I Bluhm 1
T Tsui 1

U. S. Army
Dept. of Armed Force Development
The Pentagon
RM. 3D463
Washington, DC 20301
Attn: Lt. Col. George Ivey 1

Naval Air Propulsion Test Center
Propulsion Technology and Project Engrg. Dept.
Trenton, NJ 08628
Attn C. J. Mangano 1

Commanding Officer
Naval Aviation Safety Center
Norfolk, VA 23511 1

Director, Naval Research Lab.
Washington, DC 20390
Attn Library, Code 2029 (ONRL) 1

Office of Naval Research
Washington, DC 20360
Attn N. Basdekas 1

Office of Navy Research
U. S. Navy
Branch Office, London
P. O Box 39 FPO, NY 09510 2

Air Force Flight Dynamics Laboratory
Wright-Patterson AFB, Ohio 45433
Attn F J. Janik, Jr., FDTR 1
R. M. Bader, FDTR 1

AF Office of Scientific Research
Aeromechanics and Energetics Div.
Arlington, VA 22209 1

AF Systems Command
Structures Division
Design Criteria Branch, Code FDTE
Wright-Patterson Air Force Base
Ohio 45433 1

National Aeronautics & Space Admin
Lewis Research Center
21000 Brookpark Rd
Cleveland, OH 44135
Attn· Albert Kaufman, M.S 77-2 5
John H. Weeks, M S 5-3 1
Warner L Stewart, M S. 3-5 1
Solomon Weiss, M. S 6-2 5
Richard H. Kemp, M S. 49-1 1
Marvin H Hirschberg, M. S 49-1 1
Reginald Pagnton, M S 500-206 1
Norman T. Musial, M. S 500-113 1
Library, M. S. 60-3 2
Report Control Office, M S. 3-19 1
Technology Utilization Office,
M. S. 3-19 1

National Aeronautics & Space Admin.
Washington, DC 20546
Attn. John H. Enders, Code R00 1
George W. Cherry, Code RD-P 1
Nelson F. Rekos, Code RLC 1
Kenneth E Hode, Code RO 1

NASA Scientific & Technical Information Facility
P O. Box 8757
Balt./Wash International Airport
MD 21240
Attn: Accessioning Dept. 40

DISTRIBUTION LIST (Cont'd)

Civil Aviation Authority
Airworthiness Division
Brabazon House
Red Hill, Surrey
England
Attn L. R Wilson
G. L. Gunstone

Ministry of Transport
Canadian Air Transportation Admin.
No. 3 Temporary Building
Wellington St.
Ottawa, Ontario
Canada
Attn D. R. Hemming
Director, Planning & Research, Air

Federal Aviation Administration
800 Independence Ave , S W.
Washington, DC 20591
Attn Robert Auburn, Code AFS-140
Elmer Briggs, Code. AFS-140
A K Forney, Code AFS-141

Federal Aviation Admin.
Engineering & Manufacturing Branch
N. Y. International Airport
Jamaica, L I., NY 11430
Attn: Lewis C Smith, Jr.
Richard Grassler, Code AFS-302
William McAdoo, Code. ARD-500
Edward B Shilke, Code. AFS-320

Federal Aviation Administration
Flight Standards Division
2300 East Devon Ave.
Des Plaines, IL 60018
Attn Lou Smith, Code: AGL-214

Federal Aviation Administration
12 New England Executive Rd
Burlington, MA 01803
Attn Robert Berman, Code ANE-214

National Transportation Safety Board
800 Independence Ave., S W.
Washington, DC 20591
Attn: Douglas Dreifus, Code BAS-31
J H. Lewis, Code. BAS-13

Aeronautical Research Associates of Princeton
50 Washington Rd.
Princeton, NJ
Attn J. C Houbolt

1 AiResearch Manufacturing Co of Arizona
1 Division of Garrett Corporation
402 South 36th Street
Phoenix, AZ 85034
Attn E. L. Wheeler
Technical Library

AVCO Space Systems Division
Lowell Industrial Park
Lowel, MA 01851
1 Attn Charles Steward

Batelle Memorial Institute
Columbus Lab.
505 King Ave
1 Columbus, OH 43201
1 Attn. S Goddard
1

The Boeing Co
Chief Engineer - Turbine
Seattle, WA 98124
Attn H Cruver

1 The Boeing Co.
1 ASG Impact Mechanics Labs.
1 Seattle, WA 98124
1 Attn. J Lundeberg

The Boeing Co.
SST Branch
Seattle, WA 98124
Attn. Robert Stoddard
1

The Boeing Co.
Commercial Airplane Group
Seattle, WA 98124
Attn. Jack N. Funk
1 Richard B Clarke, MS 78-81
Technical Library

Continental Aviation & Engineering Corp
Advanced Design and Materials Technology
1 12700 Kercheval Ave
1 Detroit, MI 48215
Attn: Douglas F. Oliver, Chief Engineer
Technical Library

DISTRIBUTION LIST

Deposits & Composites, Incorp
1821 Michael Faraday Dr
Reston, VA 22090
Attn Richard E Engdahl 1

Douglas Aircraft Co.
3855 Lakewood Boulevard
Long Beach, CA 90801
Attn R Kwai 1
Technical Library 1

Ford Motor Co
Industrial Engine & Turbine Operations
P O Box 2053
Dearborn, MI 48121
Attn Wm W. Sick 1
Technical Library 1

Ford Motor Company
Turbine Engineering Dept
P O. Box 2053
Dearborn, MI 48121
Attn· G Peitsch 1

General Electric Co.
Structures Design
Cincinnati, OH 45315
Attn Paul Arszman, Building 500,
Maildrop K127 1
Technical Library 1

General Electric Co.
TF30/CF6/LM2500 Low Pressure
Structures Design
Cincinnati, OH 45215
Attn: David P. Moriarty, Building 500
Maildrop K127 1

General Electric Co.
CF6 Engine Structures & Containment Design
Aircraft Engine Group
Cincinnati, OH 45215
Attn: J G. Simon 1

General Electric Co
Advanced Engrg and Tech. Programs Dept.
Aircraft Engine Group
Cincinnati, OH 45215
Attn R. H Andersen 3

General Electric Co.
1000 Western Ave
Lynn, MA 01905
Attn: Martin Van Duyn 1
Technical Library 1

General Electric Co
Space Sciences Lab
Valley Forge Space Tech Center
P O Box 8555
Philadelphia, PA 19101
Attn A P Coppa 1
Technical Library 1

General Motors Corp
Allison Division
340 White Rover Parkway
Indianapolis, IN 46206
Attn V. W. Peterson 1
Technical Library 1

General Motors Corporation
Manufacturing Development
Materials & Structures Laboratory
Warren, MI 48090
Attn S. G. Babcock 1

Hamilton Standard
Div. of United Aircraft Corp
Windsor Locks, CT 06096
Attn. R. M Stevens 1
Technical Library 1

Kaman-Avidyne
83 Second Ave.
Northwest Industrial Park
Burlington, MA 01803
Attn: N P Hobbs 1
E S. Criscione 1

DISTRIBUTION LIST (Cont'd)

Lockheed-California Co.
L 1011 Structures
Burbank, Calif. 91503
Attn Warren Stauffer, Bldg 90 1

Lockheed-California Co.
Div. of Lockheed Aircraft Corp
Burbank, CA 91503
Attn: E J. Versaw 1
Technical Library 1

McDonnell-Douglas Corporation
Missiles and Space Division
5301 Bolsa Ave
Huntington Beach, CA 92647
Attn: R. Reck 1
A J Cwiertny, Jr 1

North American Rockwell Corp.
Aerospace & Systems Group
6633 Canoga Ave.
Canoga Park, CA 91304
Attn Robert L Binsley, Dept. 841, BA42 1
Technical Library 1

Northrop Corporation
Aircraft Division
3901 West Broadway
Hawthorne, CA 90250
Attn M. J Jacobson, Dept 3761/62 1
J Brass 1
Technical Library 1

Safety Research Information Service
Research Dept.
Nat'l Safety Council
425 North Michigan Ave.
Chicago, IL 60611
Attn: Therese A Quirk 1

Sandia Corporation
Albuquerque, NM 87115
Attn. Inform Distr. Division 1
T A. Duffey 1
W. Herrmann 1
S W. Key 1
R D Krieg 1
D. E. Munson 1

Solar
Div of the International Harvester Co.
2200 Pacific High
San Diego, CA 92101
Attn: P G. Carlson
Technical Library

Southwest Research Institute
8500 Culebra Rd.
San Antonio, TX 78206
Attn. W E Baker

British Aircraft Corp Ltd
Commercial Aircraft Division
GPO Box 77
Filton House
Bristol BS 99 7AR
England
Attn· J Wallin, Chief Propulsion
Engineer